INSIGHTS

How microbes reduce sulfur p. 1476 ▸

Memory networks p. 1477

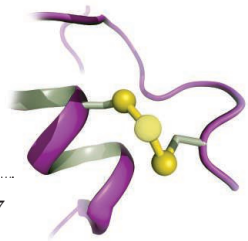

PERSPECTIVES

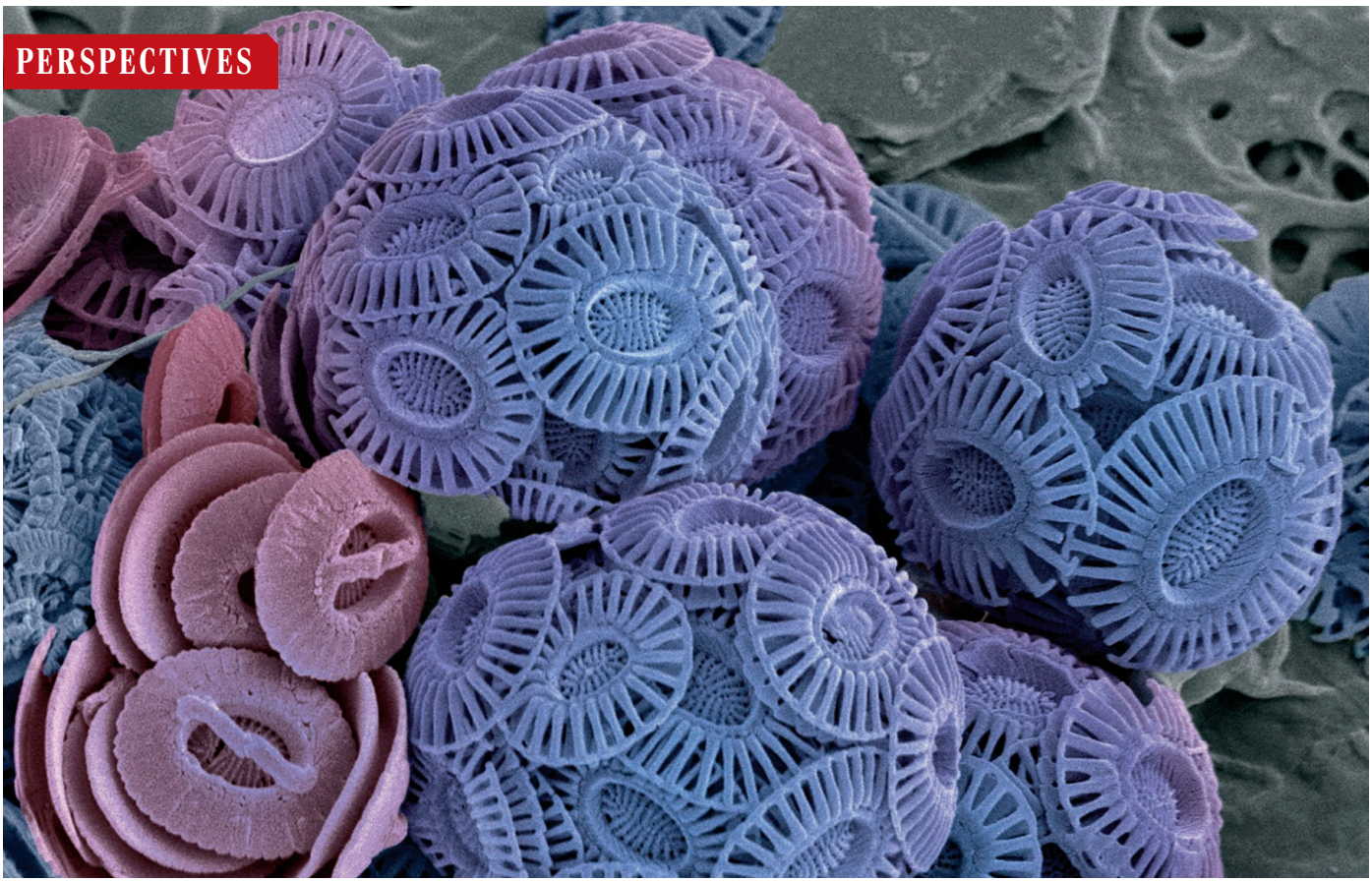

Climate-related phytoplankton habitat shifts. Colored scanning electron micrograph of the calcium carbonate shells of coccolithophores. Each plate is about ~2.5 μm wide. Ranges and abundances of this and other phytoplankton groups shift with changing ocean conditions.

PHOTO: STEVE GSCHMEISSNER/SCIENCE SOURCE

ECOLOGY

Adrift in an ocean of change

Rising temperatures and ocean acidification drive changes in phytoplankton communities

By **Meike Vogt**

Phytoplankton communities play a key role in the global biogeochemical cycling of many essential chemical elements by fixing carbon, nitrogen, and other nutrients into their biomass. If today's oceans were devoid of life, atmospheric CO_2 concentrations would be much higher than currently observed. As marine biologists strive to uncover present plankton distribution and diversity (*1*, *2*), evidence is accumulating that phytoplankton assemblages are already being affected by global change (*3*). In this issue, Rivero-Calle *et al.* (page 1533) (*4*) and McMahon *et al.* (page 1530) (*5*) use observational records of phytoplankton communities from two ocean basins to document climate-related shifts in phytoplankton communities and their environmental drivers on time scales of several decades to millennia (see the figure). The results may have implications for future ocean carbon uptake and storage.

In the realm of phytoplankton, the Who's Who is of critical importance to ecosystem function. Different phytoplankton groups have evolved various physiological strategies that allow them to thrive in marine environments ranging from freezing, nutrient-rich polar waters to warm, nutrient-poor subtropical ocean deserts. Their extensive functional diversity allows them to differentially influence global biogeochemical cycles through a variety of cellular processes that transform, store or metabolize nutrients such as nitrogen, phosphorus and carbon. For example, coccolithophores build calcium carbonate shells, influencing the ocean's carbonate chemistry and carbon export patterns (*4*). Diazotrophs fix atmospheric nitrogen during growth, thus increasing the ocean's nutrient reservoirs, marine productivity, and the efficiency of carbon export (*5*). As the climate changes,

Published by AAAS

the ranges and abundances of these and other functional groups of phytoplankton will shift. The consequences for marine ecosystem functioning and global biogeochemical cycles are as yet poorly quantified.

Despite the importance of these functional groups, little is known about their past and present distributions (*6*). Few long-term time series of pelagic phytoplankton community composition exist, because phytoplankton sampling is costly and laborious and many ocean regions are vast and remote. Laboratory studies often focus on monocultures of a few strains and thus cannot fully capture ecosystem responses, in which physiological changes at the individual level are inextricably linked to changes in the relative fitness of different taxa in a changing environment.

Shedding light on the drivers and consequences of past changes in phytoplankton communities may help us to understand their responses to future climate change. Rivero-Calle *et al.* combine long-term monitoring data with a sophisticated statistical modeling approach to show that coccolithophore abundance has increased significantly over the past five decades in the North Atlantic. They suggest that CO_2 is the primary driver of this pattern.

A preceding study based on a similar statistical model and a subset of the same dataset recorded similar coccolithophore trends, but identified temperature rather than pCO_2 as the main driver of the increase (*7*). Given that CO_2 and temperature simultaneously affect phytoplankton growth and competition, isolating their individual effects on phytoplankton physiology and competition is challenging at the ecosystem level.

Rivero-Calle *et al.* use a synthesis of published coccolithophore growth rates as a function of CO_2 and temperature to disentangle the effect of both drivers. They show that changes in temperature alone are too small to explain the magnitude of the change in coccolithophore prevalence, but that the increase is consistent with a higher growth rate due to the effect of CO_2. Linking basin-scale ecological changes to physiological changes at the cell level, this innovative study provides new evidence for a substantial reorganization of North Atlantic phytoplankton communities.

The North Atlantic is not the only basin experiencing major phytoplankton regime shifts. McMahon *et al.* reveal three different plankton regimes that succeeded each other over the past millennium in the North Pacific subtropical gyre. The authors analyzed the elemental composition of the skeletons of long-lived deep-sea corals. The skeletons record the coral's past diet of phytoplankton detritus and serve as a long-term archive of the surface phytoplankton community composition. Each regime shift identified by McMahon *et al.* coincided with major climatic changes. With the onset of the industrial era, the plankton community transitioned from a mixed community of eukaryotes and non-nitrogen–fixing cyanobacteria to one characterized by an increased contribution of diazotrophs.

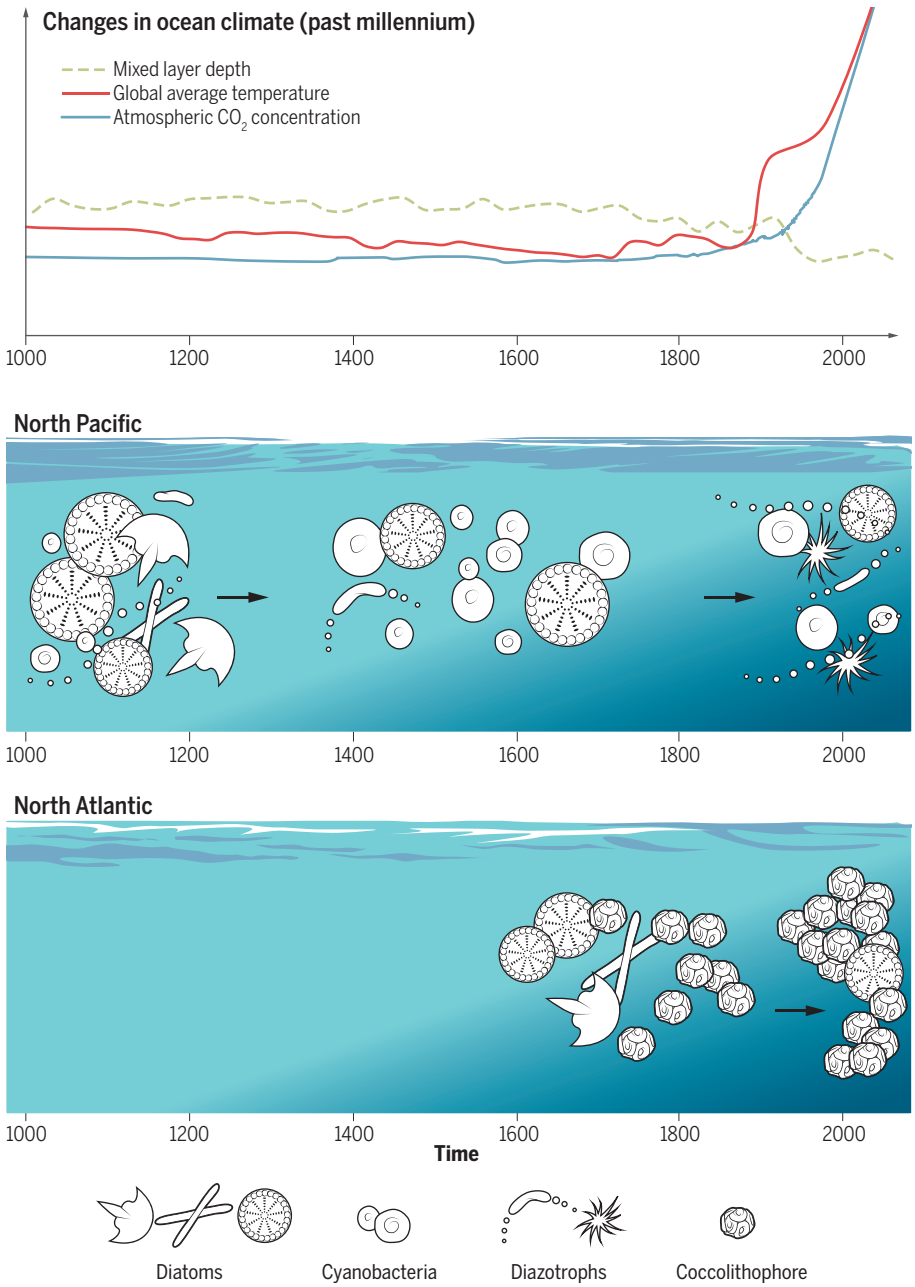

Phytoplankton trends. With rising CO_2 concentrations and temperatures, McMahon *et al.* find evidence of subtropical North Pacific phytoplankton communities shifting from non-nitrogen fixing to nitrogen-fixing, cyanobacteria-dominated phytoplankton communities during the past millennium. In the North Atlantic, Rivero-Calle *et al.* detect an increase in the relative abundance of coccolithophores in temperate and subtropical phytoplankton communities over recent decades.

McMahon *et al.* attribute the trend in diazotroph abundance to increasing sea surface temperature, stratification, and decreasing nutrient availability but do not rank these environmental drivers and do not discuss CO_2. Laboratory studies have shown that the growth of nitrogen-fixing cyanobacteria is favored under high-CO_2 conditions (*8*). Over the past millennium, changes in ocean pCO_2 were small and thus unlikely to drive the documented regime shifts, but global warming and ocean acidification may well act in

Institute for Biogeochemistry and Pollutant Dynamics, ETH Zurich, Zurich, Switzerland. E-mail: meike.vogt@env.ethz.ch

concert to restructure future Pacific phytoplankton communities.

A recent modeling study lends further support to the suggestion that CO_2 might equal or even outrank temperature in its potential to alter future phytoplankton communities. Using a complex global marine ecosystem model, Dutkiewicz *et al.* simulated phytoplankton community structure under global warming and ocean acidification over the 21st century (*9*). Differing growth responses of the phytoplankton types to increased pCO_2 caused substantial shifts in simulated phytoplankton communities, with global increases in both coccolithophore and diazotroph biomass.

Regardless of the main drivers, the species and regime shifts in the phytoplankton communities are likely to alter ocean biogeochemistry. Yet, the relationships between community structure and ocean biogeochemistry are poorly understood, and current evidence suggests that they will depend on the spatiotemporal scales at which they are considered. For example, several long-term studies have reported a negative correlation between past coccolithophore calcification rates and CO_2 levels (*10*, *11*). However, a short-term laboratory study simulating future conditions has identified a few coccolithophore species with impressive adaptive capabilities, providing a compensation mechanism for rising CO_2 (*12*).

As climate change is altering marine ecosystems at an unprecedented rate, research efforts must address the link between marine ecosystem function and phytoplankton biogeography. Further insight will require integration of in situ, satellite, and palaeoceanographic observations with laboratory studies and modeling. Data limitation continues to be the most pressing problem for monitoring large-scale species and regime shifts. Even though the environment in which they live will undergo substantial changes, phytoplankton evolved billions of years ago and are likely to stay afloat in the changing seas. The question is how higher trophic level organisms, such as us, will deal with changes in the services that plankton ecosystems provide. ■

REFERENCES

1. C. de Vargas *et al.*, *Science* **348**, 1261605 (2015).
2. S. Sunagawa *et al.*, *Science* **348**, 6237 (2015).
3. P. Reid *et al.*, *Nature* **391**, 546 (1998).
4. S. Rivero-Calle *et al.*, *Science*, **350**, 1533 (2015).
5. K. W. McMahon *et al.*, *Science* **350**, 1530 (2015).
6. E. Buitenhuis *et al.*, *Earth Sys. Sci. Data* **5**, 227 (2013).
7. G. Beaugrand *et al.*, *Nat. Climate Change* **3**, 263 (2013).
8. D. Hutchins *et al.*, *Nat. Geosci.* **6**, 790 (2015).
9. S. Dutkiewicz *et al.*, *Nat. Climate Change* **5**, 1002 (2015).
10. S. O'Dea *et al.*, *Nat. Commun.* **5**, 5363 (2014).
11. L. Beaufort *et al.*, *Nature* **476**, 80 (2011).
12. L. Schlüter *et al.*, *Nat. Climate Change* **4**, 1024 (2014).

10.1126/science.aad6946

MATERIALS SCIENCE

Disclosing boron's thinnest side

Borophene—stable, single-atom-thick layers of boron—displays remarkable properties

By **Hermann Sachdev**[1,2]

Current research on two-dimensional (2D) materials like graphene, boronitrene layers, phosphorene, silicene, or transition-metal dichalcogenides is focused on the tuning of their electronic and photonic properties combined with high-quality film syntheses. Major goals are the fabrication of (semi)-conducting films for nanoscale electronic devices and applications to improve the performance of energy conversion and storage systems (*1*–*4*). The mechanical properties of graphene and MoS_2 are also being considered for their nano- and mesoscale tribological aspects (*5*). On page 1513 of this issue, Mannix *et al.* (*6*) report on the formation of atomically thin boron films—borophene—by the evaporation and deposition of boron on a Ag(111) surface. The position of boron in the periodic system, between metallic beryllium and nonmetallic carbon, classifies it as a semimetal. Boron displays a pronounced ability to form not only strong covalent two-center-two-electron bonds, but also stable electron-deficient three-center-two-electron bonds. This results in a manifold of 3D cluster patterns for the solid-state structures of elemental boron polymorphs. The strong covalent bonds are responsible for boron and structurally related borides being hard materials. Also, no other p-block element shows a similar complexity of chemical bonding, which is as well displayed within the cluster chemistry of boron hydrides and carboranes (*7*).

"...single and multiple borophene layers offer a broad perspective for the development of nanoscale electronic devices..."

Mannix *et al.* characterized the boron monolayers by scanning tunneling microscopy and low-energy electron diffraction and found that they display a remarkable similarity to a model for "borophene," a quasiplanar molecular compound consisting of a B_{36} cluster of boron atoms (*8*). The dominant pattern of this molecular structure exhibits a hexagonal array of boron atoms with an additional boron atom located centrally within each B_6 hexagon. Because no alloying with the underlying silver substrate is observed, the single atom thick layer of boron can be considered as a novel 2D boron polymorph. Owing to the strong covalent interactions within this 2D borophene layer, the structure resembles a missing link between fully covalent bound 2D materials (graphene, boronitrene layers, phosphorene) and support-stabilized semimetallic films of single atomic thickness like silicene and germanene.

Depending on the relative orientation of the boron monolayer to the Ag(111) substrate and the deposition conditions, different domain structures can be distinguished. These structures can be derived from a corrugated hexagonal array of boron atoms, with additional boron atoms located above each center of a six-membered ring (see the figure), with distortions imposed by the substrate symmetry leading to ribbonlike structural features (*6*). Like benzene (C_6H_6) for graphene, a B_7 molecular cluster (being formed by boron evaporation and stable as per calculations) can be formally regarded as an elemental structure of the borophene layer.

In situ electronic characterization by scanning tunneling spectroscopy reveals anisotropic metallic characteristics, with the electronic conductivity correlating to the chainlike superstructures according to density-of-state calculations. Borophene layers are more stable than silicene layers, owing to the strong covalent interactions of boron atoms by multicenter electron-deficient bonds, but still display a considerable reactivity, e.g., toward oxygen. The borophene structure could be successfully stabilized with a Si/SiO_x buffer layer for exposure at ambient conditions, as indicated by transmission electron microscopy.

These films give rise to considerable toughness, in addition to their structural and electronic properties. Calculations reveal an in-plane Young's modulus in correlation with the experimentally observed structural anisotropy of the boron epilayer (398 GPa·nm

[1]*Max Planck Institute for Polymer Research, Ackermannweg 10, D-55128 Mainz, Germany.* [2]*Technische Universität Kaiserslautern, Abt. Mechanische Verfahrenstechnik/Particle Process Engineering, Gottlieb-Daimler-Straße Geb. 44, D-67663 Kaiserslautern, Germany. E-mail: sachdev@mpip-mainz.mpg.de; hermann.sachdev@mv.uni-kl.de*

PHYTOPLANKTON

Millennial-scale plankton regime shifts in the subtropical North Pacific Ocean

Kelton W. McMahon,[1,2]* Matthew D. McCarthy,[1] Owen A. Sherwood,[3] Thomas Larsen,[4] Thomas P. Guilderson[1,2,5]

Climate change is predicted to alter marine phytoplankton communities and affect productivity, biogeochemistry, and the efficacy of the biological pump. We reconstructed high-resolution records of changing plankton community composition in the North Pacific Ocean over the past millennium. Amino acid–specific $\delta^{13}C$ records preserved in long-lived deep-sea corals revealed three major plankton regimes corresponding to Northern Hemisphere climate periods. Non–dinitrogen-fixing cyanobacteria dominated during the Medieval Climate Anomaly (950–1250 Common Era) before giving way to a new regime in which eukaryotic microalgae contributed nearly half of all export production during the Little Ice Age (~1400–1850 Common Era). The third regime, unprecedented in the past millennium, began in the industrial era and is characterized by increasing production by dinitrogen-fixing cyanobacteria. This picoplankton community shift may provide a negative feedback to rising atmospheric carbon dioxide concentrations.

Gone is the paradigm of the oligotrophic subtropical gyres as vast oceanic deserts. In the recent instrumental record, a new picture has emerged of substantial dynamics in plankton community structure, biogeochemical cycling, and export production (*1*–*4*). Numerous lines of evidence suggest that shifts in phytoplankton community regimes are intimately connected to oceanographic conditions (*2*, *4*, *5*). For instance, the 1976 polarity reversal of the Pacific Decadal Oscillation caused a shoaling of the mixed layer and subsequent declines in available nutrients to the North Pacific Subtropical Gyre (NPSG); these conditions probably promoted the food-web regime shift from a eukaryotic to a prokaryotic, cyanobacteria-dominated system (*2*). Such changes are superimposed on secular shifts associated with the areal increase of subtropical gyres that has been ongoing for at least 25 years (*6*). In the face of increasing climate change, it is imperative to understand recent changes at the base of the NPSG food web in the context of longer-term trends. However, our understanding of how NPSG plankton communities have shifted on centennial time scales has been limited by a lack of available methods and paleoarchives of sufficient length and resolution.

Hawaiian gold corals (*Kulamanamana haumeaae*) are extraordinarily long-lived deep-sea organisms that record the biogeochemical signatures of recently exported production in their proteinaceous skeletons (*7*, *8*). We generated millennial-length records of bulk stable carbon isotopes ($\delta^{13}C_{bulk}$) from specimens of *K. haumeaae* collected from the top of the mesopelagic zone at two sites in the Hawaiian archipelago (Fig. 1). The $\delta^{13}C_{bulk}$ records showed remarkable congruence, characterized by a gradual increase of ~1.0 per mil (‰) from ~1000 to ~1850 CE, followed by a rapid decrease of –1.0‰ from ~1850 to the present, after correcting for the Suess effect (Fig. 2A) (*9*–*11*). These changes in $\delta^{13}C_{bulk}$ imply multicentennial-scale shifts in $\delta^{13}C$ values associated with primary production, which we hypothesize reflect major changes in plankton community structure over the past 1000 years.

Bulk $\delta^{13}C$ records integrate the combined influences of the $\delta^{13}C$ value of inorganic carbon utilized during carbon fixation, shifts in plankton community structure, trophic changes, and biochemical fractionation. To isolate plankton source signatures within this signal, we applied a powerful fingerprinting approach to the sampled deep-sea corals, based on the normalized $\delta^{13}C$ values of essential amino acids ($\delta^{13}C_{EAA}$) in primary producers (*11*). These $\delta^{13}C_{EAA}$ fingerprints reflect the substantial metabolic diversity in EAA synthesis pathways and associated isotope effects among evolutionarily distinct primary producers (*12*, *13*). We found diagnostic multivariate patterns in literature values of normalized $\delta^{13}C_{EAA}$ among four key source end-members relevant to the NPSG [eukaryotic microalgae, dinitrogen (N_2)–fixing and non–N_2-utilizing cyanobacteria, and heterotrophic bacteria] (fig. S2). Because animals cannot synthesize the carbon skeletons of EAAs (*14*), these $\delta^{13}C_{EAA}$ fingerprints are incorporated, virtually unmodified, into upper-trophic-level consumers, including gorgonin corals (*15*). Furthermore, $\delta^{13}C_{EAA}$ fingerprints are robust to the many factors affecting bulk $\delta^{13}C$ values, such as environmental and growth conditions (*13*, *16*).

A subset of the deep-sea coral samples spanning the entire 1000-year record was analyzed for $\delta^{13}C_{EAA}$ at ~20-year resolution (table S1). $\delta^{13}C_{EAA}$ values were strongly correlated with $\delta^{13}C_{bulk}$ (fig. S1), indicating that trends in $\delta^{13}C_{bulk}$ can be attributed to changes in source carbon at the base of the food web (*15*). For example, the $\delta^{13}C_{EAA}$ of

[1]Department of Ocean Sciences, University of California–Santa Cruz, Santa Cruz, CA 95064, USA. [2]Institute for Marine Sciences, University of California–Santa Cruz, Santa Cruz, CA 95064, USA. [3]Institute of Arctic and Alpine Research, University of Colorado–Boulder, Boulder, CO 80309, USA. [4]Leibniz Laboratory for Radiometric Dating and Stable Isotope Research, Christian-Albrechts-Universität zu Kiel, 24118 Kiel, Germany. [5]Lawrence Livermore National Laboratory, Livermore, CA 94550, USA.
*Corresponding author. E-mail: kemcmaho@ucsc.edu

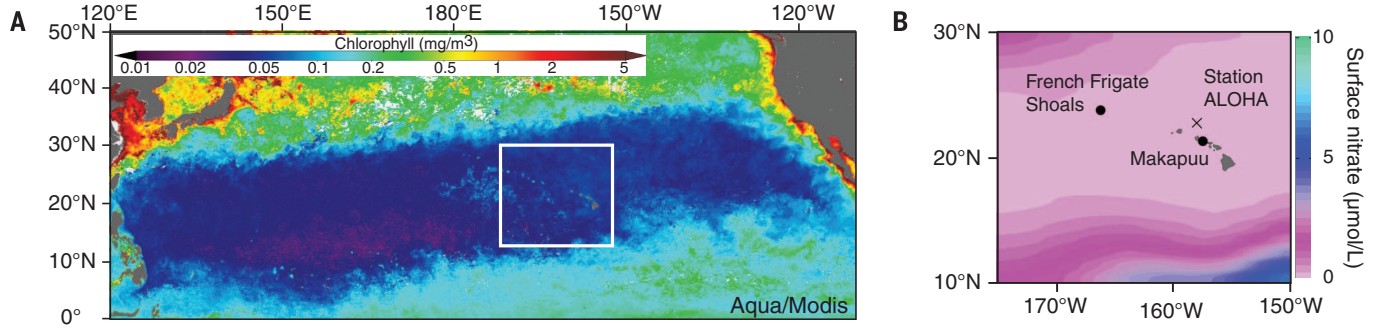

Fig. 1. NPSG productivity distribution, with sample locations. (**A**) Spatial extent of the oligotrophic NPSG, determined from spring 2012 chlorophyll a concentrations measured remotely by NASA's Aqua/MODIS (Moderate Resolution Imaging Spectroradiometer). The white box indicates the area shown in (B). [Image courtesy of NASA Goddard's Ocean Biology Processing Group] (**B**) *K. haumeaae* sampling locations at Makapuu and French Frigate Shoals relative to the oceanographic station ALOHA (indicated by the X), overlain on ocean surface nitrate concentrations (National Oceanographic Data Center, 2013; https://www.nodc.noaa.gov/cgi-bin/OC5/woa13/woa13oxnu.pl?parameter=n).

phenylalanine (Fig. 2B) mirrored that of $\delta^{13}C_{bulk}$ (Fig. 2A); however, the magnitude of change was 10 times larger than in $\delta^{13}C_{bulk}$. This suggests that isotopic contributions from other macromolecules had a strong muting effect on $\delta^{13}C_{bulk}$ values, and thus $\delta^{13}C_{EAA}$ is likely a more sensitive record of changes in primary producer $\delta^{13}C$ than $\delta^{13}C_{bulk}$ is (*15*). Our results indicate that variability in $\delta^{13}C$ values of exported production was much larger than would be inferred from coral $\delta^{13}C_{bulk}$ records alone, and strongly suggest broad changes in the sources of exported primary production through time.

To reconstruct past shifts in the relative contributions of major phytoplankton groups to export production in the NPSG, we applied a Bayesian stable isotope–mixing model to published source end-member $\delta^{13}C_{EAA}$ fingerprints (*11*) and the $\delta^{13}C_{EAA}$ records of *K. haumeaae*, normalized to their respective means (fig. S2 and table S2). Over the entire 1000-year record, photoautotrophic carbon dominated the corals' sinking particulate organic matter (POM) food source (mean, 87 ± 6%), with a relatively small heterotrophic bacterial contribution (13 ± 6%) (Fig. 3). Likewise, prokaryotic cyanobacterial sources dominated photoautrophic carbon (63 ± 14%), with a moderate mean contribution from eukaryotic microalgae (24 ± 10%) (Fig. 3). On centennial time scales, however, relative contributions from photoautotrophic end-members shifted dramatically. For example, between 1000 and 1850 CE, cyanobacteria decreased from 80 to 50% of total exported production, offset by an equivalent increase in eukaryotic microalgae up to a peak contribution of ~45% in the early 1800s. Although previous studies have noted enhanced diatom abundances in the NPSG associated with mesoscale oceanographic features (*17*), such a sustained high level of eukaryotic microalgal production has never been observed in the modern instrumental record. The most conservative explanation of our data is that the changes in the phylogenetic identity of sources contributing to export production reflect changes in the relative community composition of surface plankton through time. An alternate, albeit highly unlikely, hypothesis is that surface plankton community composition has remained relatively constant through time, and instead the degree of decoupling between surface and export production has undergone dramatic changes as a function of climate shifts (*11*).

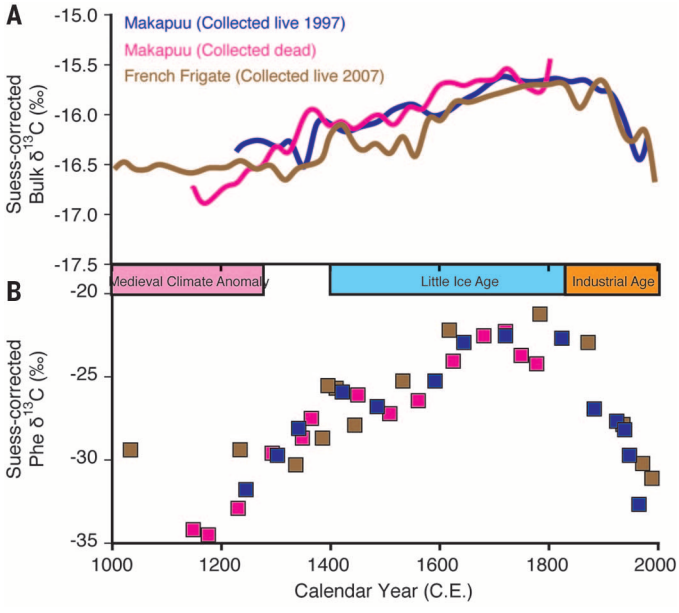

Fig. 2. 1000-year bulk and essential amino acid $\delta^{13}C$ records from deep-sea corals in the NPSG. *K. haumeaae*–derived records of (**A**) $\delta^{13}C_{bulk}$ (solid lines show the 20-year average; analytical error, 0.05‰) and (**B**) $\delta^{13}C_{Phe}$ (Phe, phenylalanine; squares; analytical error, 0.2‰) from Makapuu live coral (purple), Makapuu fossil coral (magenta), and French Frigate Shoals live coral (brown). All records have been corrected for the oceanic Suess effect since 1860 (*10*, *11*). Well-known Northern Hemisphere climate phenomena are overlaid for reference (*18*).

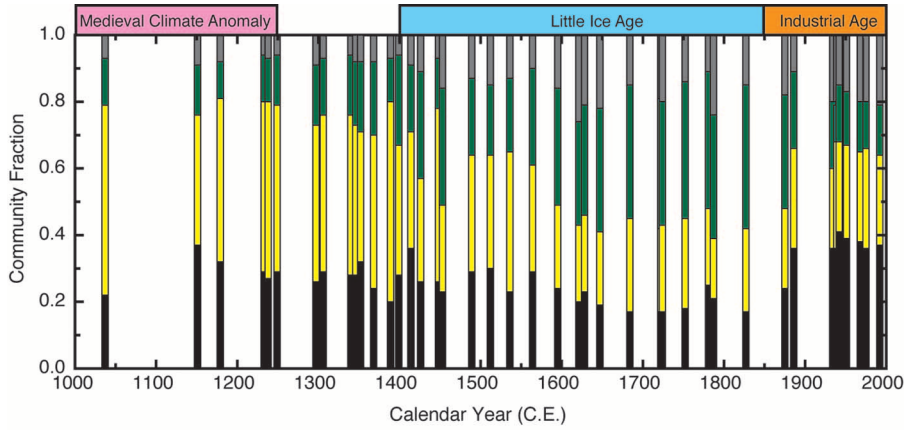

Fig. 3. Millennial record of relative carbon contributions from different primary producers recorded in deep-sea corals. Shown are the relative contributions of carbon from N_2-fixing cyanobacteria (black), non–N_2-utilizing cyanobacteria (yellow), eukaryotic microalgae (green), and heterotrophic bacteria (gray), recorded in deep-sea corals over the past 1000 years. Corals were collected at 450 m depth in the Hawaiian archipelago in the NPSG. Relative contributions are based on a compound-specific Bayesian stable isotope–mixing model of normalized phytoplankton end-member and coral $\delta^{13}C_{EAA}$ values.

To better constrain the patterns of changing plankton community composition, we applied a hierarchical cluster analysis to the normalized $\delta^{13}C_{EAA}$ data (*11*). This approach identified three distinct plankton community regimes that corresponded temporally to well-known Northern Hemisphere climate phenomena (Fig. 4). The first regime corresponded to the Medieval Climate Anomaly [MCA; 950–1250 CE (*18*)], with $\delta^{13}C_{EAA}$ fingerprints indicative of export production dominated by nitrate (NO_3^-)–utilizing cyanobacteria. There is general consensus that the putative MCA in the northern mid-latitudes was similar to the climate of the mid-20th century (*18*, *19*), implying relatively warm sea surface temperatures, weak winds, shallow mixed-layer depths, and resultant nutrient limitation, all favoring a microbial loop–dominated community (*2*). The second regime corresponded to the Little Ice Age [LIA; 1400–1850 CE (*18*)]. In this regime, the plankton assemblage contributing to export production transitioned from a cyanobacteria-dominated community to one far more strongly influenced by eukaryotic microalgae (Fig. 3). This shift probably reflects a transition in the LIA to cooler sea surface temperatures, a reduction in stratification, an increase in mixed-layer depth, and an inferred increase in the supply of inorganic nitrate from depth (*4*, *20*).

The third and current regime began at the end of the LIA and at the onset of the modern industrial age (~1850 CE) (Fig. 4). This regime is distinguished by a transition back to a cyanobacteria-dominated system. However, unlike the MCA period, the current regime is characterized by a biogeochemically distinct group of cyanobacteria, the N_2-fixing diazotrophs. Historically, the availability of inorganic nitrogen (N) and/or phosphorus (P) was thought to limit plankton production in the NPSG (*21*). Since ~1850 CE, however, sea surface temperatures have increased, accompanied by a likely decrease in the trade winds concomitant with gyre expansion, as a result of Northern Hemisphere warming. The resulting increase in stratification and decrease in nutrient availability may have selected for a N_2-fixing cyanobacterial community, as observed in the instrumental record over

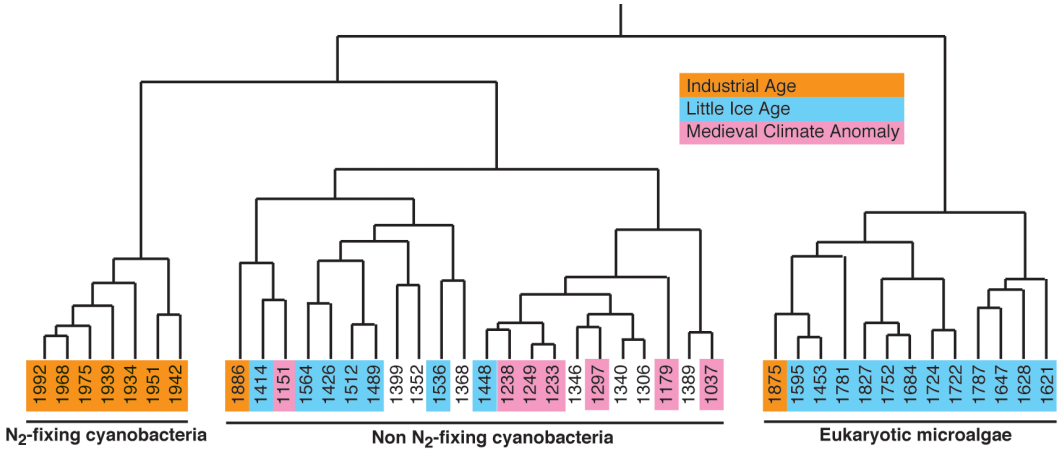

Fig. 4. Phytoplankton regime shifts recorded in deep-sea corals. Shown is a dendrogram of similarity in exported plankton carbon utilized by deep-sea corals over the past 1000 years, based on an average-link hierarchical cluster analysis. The dendrogram is separated into three significantly different clusters according to multiscale bootstrapping with approximately unbiased *P* values >0.95. The dates (CE) are colored based on overlap with well-known Northern Hemisphere climate phenomena (*18*).

the past ~20 years (*2*, *22*). Currently declining P inventories and increasing N:P ratios in the mixed layer at the HOT-ALOHA (Hawaiian Ocean Time-series–A Long-Term Oligotrophic Habitat Assessment) oceanographic station are thought to reflect this decades-long increase in N_2 fixation (*1*, *2*, *8*), an idea that is further supported by recent literature suggesting that canonical Redfield ratios in the NPSG may be more plastic than previously realized (*23*, *24*).

Our $\delta^{13}C_{EAA}$ fingerprinting data, which show a 47% increase in N_2-fixing cyanobacteria carbon in exported POM since the end of the LIA, correspond well with recent evidence of a 17 to 27% increase in NPSG N_2-fixation since ~1850 CE, determined from amino acid–specific nitrogen isotopes ($\delta^{15}N_{AA}$) in the same suite of *K. haumeaae* specimens as used in this study (*8*). These studies represent fully independent lines of evidence supporting the hypothesis that recent decreases in $\delta^{15}N_{bulk}$ values of exported POM in the NPSG are related to increases in diazotrophic plankton within a microbial loop–driven system (*11*).

By offering the first direct phylogenetic context for long-term shifts in isotopic records of exported POM, our data provide a major new constraint in understanding the evolution of NPSG biogeochemistry. For example, a recently proposed alternate hypothesis contends that advection of ^{15}N-depleted nitrate from the Eastern Tropical Pacific, associated with a reduction in denitrification (*25*), might explain recent low $\delta^{15}N$ values in the NPSG; similarly, Kim *et al.* (*26*) suggested that atmospheric N deposition is the dominant factor driving increases in values of N* (a nitrate- and phosphate-based tracer of N_2 fixation and denitrification) across the Pacific. However, the $\delta^{15}N$ value of N entrained in the mixed layer should not, by itself, affect planktonic community structure. Our new evidence for a profound phylogenetic community shift is fully consistent with increasing N_2 fixation, probably linked to overall increased stratification and reductions in upwelled nitrate, over the past 100 years.

Taken together, our data show that phytoplankton community structure in the NSPG is subject to multicentennial shifts that are broadly linked to climate conditions. They also reveal that the present-day cyanobacterial community, which is characterized by strongly enhanced N_2 fixation, is unprecedented within at least the past 1000 years. The transition to the current cyanobacterial regime (<200 years) was much faster than the transition from cyanobacterial dominance during the MCA to eukaryotic dominance during the LIA (>600 years). Both the nature and the rate of change of the current dominant autotrophic assemblage strongly suggest continuing rapid changes in NPSG plankton community structure associated with anthropogenic climate change and are consistent with the predicted expansion of N_2-fixing cyanobacteria habitat (*27*).

Regime shifts in plankton community composition have far-reaching implications for productivity, food-web dynamics, biogeochemical cycling, and the efficacy of the biological pump (*22*, *28*, *29*). The fact that dominant cyanobacterial signatures were recorded in deep-sea corals from the mesopelagic zone strongly suggests that continuing shifts to an N_2-fixing prokaryotic regime have fundamentally altered the main sources of exported POM. These observations also support recent evidence (*3*, *30*) that small-cell picoplankton production, free-living and/or in cyanobacteria-diatom symbioses (*11*, *22*), may be a more important component of export production in oligotrophic gyres than traditionally recognized. Further, recent studies have shown that plankton elemental stoichiometry is more variable than previously assumed under the classical Redfield paradigm, with C:P ratios being several times higher in the oligotrophic gyres than in upwelling regions (*23*, *24*). This suggests that carbon export could actually be more efficient (per mole of P) in the oligotrophic gyres, despite their lower overall productivity, and, furthermore, that increasing nutrient limitation in warmer and more stratified oceans over the past 100 years may have served as a major negative feedback on rising CO_2 concentrations (*23*, *24*). Our finding that the phylogenetic origin of export production in the NPSG has trended toward N_2-fixing prokaryotes over the past century strongly supports this idea. If small-cell export does in fact act as a more efficient carbon pump, our new records suggest that this carbon cycle feedback has already been operating for the past 100 years. For this feedback loop to persist into the future, the system cannot become phosphate-limited.

REFERENCES AND NOTES

1. D. M. Karl, *Ecosystems* **2**, 181–214 (1999).
2. D. M. Karl, R. R. Bidigare, R. M. Letelier, *Deep Sea Res. Part II Top. Stud. Oceanogr.* **48**, 1449–1470 (2001).
3. T. L. Richardson, G. A. Jackson, *Science* **315**, 838–840 (2007).
4. J. E. Dore, R. M. Letelier, M. J. Church, R. Lukas, D. M. Karl, *Prog. Oceanogr.* **76**, 2–38 (2008).
5. G. C. Hays, A. J. Richardson, C. Robinson, *Trends Ecol. Evol.* **20**, 337–344 (2005).
6. J. J. Polovina, E. A. Howell, M. Abecassis, *Geophys. Res. Lett.* **35**, L03618 (2008).
7. T. P. Guilderson, M. D. McCarthy, R. B. Dunbar, A. Englebrecht, E. B. Roark, *Biogeosciences* **10**, 6019–6028 (2013).
8. O. A. Sherwood, T. P. Guilderson, F. C. Batista, J. T. Schiff, M. D. McCarthy, *Nature* **505**, 78–81 (2014).
9. R. J. Francey *et al.*, *Tellus B Chem. Phys. Meteorol.* **51**, 170–193 (1999).
10. P. Quay, R. Sonnerup, T. Westby, J Stutsman, A. McNichol, *Global Biogeochem. Cycles* **17**, 4-1–4-20 (2013).
11. Materials and methods are available as supplementary materials on *Science* Online.
12. J. H. Scott *et al.*, *Astrobiology* **6**, 867–880 (2006).
13. T. Larsen *et al.*, *PLOS ONE* **8**, e73441 (2013).
14. K. W. McMahon, L.-L. Hamady, S. R. Thorrold, *Oceanogr. Mar. Biol. Annu. Rev.* **51**, 327–374 (2013).
15. J. T. Schiff *et al.*, *Mar. Chem.* **166**, 82–91 (2014).
16. T. Larsen *et al.*, *Biogeosciences* **12**, 4979–4992 (2015).
17. R. Scharek, M. Latasa, D. M. Karl, R. R. Bidigare, *Deep Sea Res. Part I Oceanogr. Res. Pap.* **46**, 1051–1075 (1999).
18. M. E. Mann *et al.*, *Science* **326**, 1256–1260 (2009).
19. V. Trouet *et al.*, *Science* **324**, 78–80 (2009).
20. G. Corno *et al.*, *J. Geophys. Res.* **112**, C04021 (2007).
21. R. W. Eppley, E. H. Renger, E. L. Venrick, M. M. Mullin, *Limnol. Oceanogr.* **18**, 534–551 (1973).
22. D. M. Karl, M. J. Church, J. E. Dore, R. M. Letelier, C. Mahaffey, *Proc. Natl. Acad. Sci. U.S.A.* **109**, 1842–1849 (2012).
23. A. C. Martiny *et al.*, *Nat. Geosci.* **6**, 279–283 (2013).
24. Y. C. Teng, F. W. Primeau, J. K. Moore, M. W. Lomas, A. C. Martiny, *Nat. Geosci.* **7**, 895–898 (2014).
25. C. Deutsch *et al.*, *Science* **345**, 665–668 (2014).
26. I. N. Kim *et al.*, *Science* **346**, 1102–1106 (2014).

27. P. Flombaum *et al.*, *Proc. Natl. Acad. Sci. U.S.A.* **110**, 9824–9829 (2013).
28. P. G. Falkowski, R. T. Barber, V. Smetacek, *Science* **281**, 200–206 (1998).
29. P. W. Boyd, P. P. Newton, *Deep Sea Res. Part I Oceanogr. Res. Pap.* **46**, 63–91 (1999).
30. H. G. Close *et al.*, *Proc. Natl. Acad. Sci. U.S.A.* **110**, 12565–12570 (2013).

ACKNOWLEDGMENTS

All methods, additional figures, and source data are available in the supplementary materials. K.W.M., T.P.G., and M.D.M. conceived the project. K.W.M. prepared samples, performed bulk and compound-specific $\delta^{13}C$ analyses, and wrote the manuscript. O.A.S. and T.L. assisted in data analysis and commented on the manuscript. T.P.G. and M.D.M. supervised this project, discussed the results, and commented on the manuscript. We thank M. Hanson, S. Fauqué, and J. Liu for assistance in the laboratory. This work would not have been possible without the captain and crew of the research vessel *Ka'imikai-o-Kanaloa* and the pilots and engineers of the Hawaii Undersea Research Laboratory's Pisces IV and V submersibles. We also thank three anonymous reviewers for valuable feedback on the manuscript. Funding for sample collection was provided by the National Oceanic and Atmospheric Administration's National Undersea Research Program and the National Geographic Society (grant 7717-04). A portion of this work was performed under the auspices of the U.S. Department of Energy (grant DE-AC52-07NA27344). The majority of the work presented here was funded by NSF (grant OCE-1061689). T.L. was supported by The Future Ocean, a program funded by the German Research Foundation.

SUPPLEMENTARY MATERIALS

www.sciencemag.org/content/350/6267/1530/suppl/DC1
Materials and Methods
Figs. S1 and S2
Tables S1 and S2
References (*31*–*68*)

25 February 2015; accepted 6 November 2015
Published online 26 November 2015
10.1126/science.aaa9942

MARINE CALCIFERS

Multidecadal increase in North Atlantic coccolithophores and the potential role of rising CO_2

Sara Rivero-Calle,[1,2]* Anand Gnanadesikan,[1]* Carlos E. Del Castillo,[1,3] William M. Balch,[4] Seth D. Guikema[5]

As anthropogenic carbon dioxide (CO_2) emissions acidify the oceans, calcifiers generally are expected to be negatively affected. However, using data from the Continuous Plankton Recorder, we show that coccolithophore occurrence in the North Atlantic increased from ~2 to more than 20% from 1965 through 2010. We used random forest models to examine more than 20 possible environmental drivers of this change, finding that CO_2 and the Atlantic Multidecadal Oscillation were the best predictors, leading us to hypothesize that higher CO_2 levels might be encouraging growth. A compilation of 41 independent laboratory studies supports our hypothesis. Our study shows a long-term basin-scale increase in coccolithophores and suggests that increasing CO_2 and temperature have accelerated the growth of a phytoplankton group that is important for carbon cycling.

Marine organisms that produce external features made of calcium carbonate are susceptible to harmful consequences from ocean acidification (*1*). Coccolithophores, the main calcifying phytoplankton, are unicellular algae surrounded by calcite plates called coccoliths, whose photosynthesis is strongly carbon-limited (*2*). Coccoliths are a major source of oceanic particulate inorganic carbon (PIC) and serve as ballast for sinking aggregates (*3*), thus accelerating carbon export (*4*). Given increasing partial pressures of atmospheric CO_2 (pCO_2), global warming, and ocean acidification, it is expected that coccolithophores will be affected, producing concomitant effects on ocean carbon fluxes, dimethyl sulfide fluxes (*5*), carbonate geochemistry (*6*), and phytoplankton community structure (*6*). Current evidence regarding how increased pCO_2 will affect coccolithophores is contradictory (*7*–*10*). Most laboratory manipulations study how coccolithophores respond to the increased pCO_2 levels predicted for the end of the century rather than to the CO_2 changes observed in the past five decades.

Here, we report changes in the occurrence of coccolithophores in the North Atlantic during the past 45 years and use random forest (RF) statistical models to evaluate the importance of various environmental drivers for these changes.

The in situ Continuous Plankton Recorder (CPR) surveys were developed to sample plankton in the North Atlantic using ships of opportunity. The surveys have followed the same methodology since 1946 (*11*). Sample preservation methods (using Borax-buffered formalin) and analysis have remained unchanged since 1958 (*12*), producing a unique, consistent, multidecadal data set. Although the CPR filtering system was designed to sample larger microplankton, coccolithophores are trapped, particularly in the intersection of the silk fibers (*12*). It is not possible to accurately quantify organisms that are smaller than the mesh size, but we can use the data set to estimate the probability of coccolithophore occurrence. Although our sampling underestimates natural abundances, this probability is a proxy for changes in coccolithophore abundance (fig. S1).

We calculated the annual probability of coccolithophore occurrence as the fraction of samples per year containing coccolithophores. The CPR data show an increase in occurrence of coccolithophores across the North Atlantic from ~2% of samples in the 1960s to more than 20% of samples with coccolithophores in the 2000s (Fig. 1, A to F, and fig. S2). Regional abundances of coccolithophores in the 2000s are at least 10 times higher than those observed at the beginning of the data record. Our observations are supported by a shift in the opal:carbonate ratio in sediment traps in the Atlantic from the 1990s (*13*), satellite evidence of global poleward expansion of *Emiliania huxleyi* (*14*), and recurring blooms in areas where coccolithophores were previously absent or sparse (*14*–*17*).

To evaluate possible top-down and bottom-up drivers for the increase in coccolithophore occurrence in the North Atlantic, we investigated factors that could affect coccolithophore growth rates and biogeography. Temperature, nutrient availability, light levels, competition, and predation are critical on a local scale. In turn, these may be affected by large-scale processes such as climate modes, global warming, and increases in CO_2. The CPR sampling survey is irregular in time and space, making classic time series analysis inappropriate for this data set. Additionally, the effects of different environmental forcings on phytoplankton groups are nonlinear and interdependent. After evaluating a suite of statistical methods (see the supplementary materials), we selected RF models (*18*), an increasingly popular method in ecology that characterizes structure in high dimensional data while making no distributional assumptions about the response variable or predictors. RF has the advantage of allowing for nonlinearities, geographically and temporally discontinuous data, and the ability to model complex interactions among predictor variables without overfitting the data.

Our RF model predicted the probability of coccolithophore occurrence, defined as the percentage of samples containing coccolithophores in a 1°-by-1° area each month, as a function of more than 20 biological and physical predictors. Because the CPR data set is already complex and discontinuous, we only used in situ measurements of biological and physical parameters without interpolating data. The complete data set included 81,340 observations from 1965 to 2010. The importance of each variable in predicting coccolithophore

[1]Department of Earth and Planetary Sciences, The Johns Hopkins University, Baltimore, MD, USA. [2]Applied Physics Laboratory, The Johns Hopkins University, Baltimore, MD, USA. [3]Goddard Space Flight Center, National Aeronautics and Space Administration, Greenbelt, MD, USA. [4]Bigelow Laboratory for Ocean Sciences, East Boothbay, ME, USA. [5]Department of Industrial and Operations Engineering, The University of Michigan, Ann Arbor, MI, USA.
*Corresponding author. E-mail: sara.rivero@jhu.edu (S.R.-C.); gnanades@jhu.edu (A.G.)

www.sciencemag.org/cgi/content/full/science.aaa9942/DC1

Supplementary Materials for

Millennial-scale plankton regime shifts in the subtropical North Pacific Ocean

Kelton W. McMahon,* Matthew D. McCarthy, Owen A. Sherwood, Thomas Larsen, Thomas P. Guilderson

*Corresponding author. E-mail: kemcmaho@ucsc.edu

Published 26 November 2015 on *Science* Express
DOI: 10.1126/science.aaa9942

This PDF file includes:

Title: Millennial-scale plankton regime shifts in the subtropical North Pacific Ocean

Authors: Kelton W. McMahon[1*], Matthew D. McCarthy[1], Owen A. Sherwood[2], Thomas Larsen[3], Thomas P. Guilderson[1,4,5]

1. Supplementary Methods and Discussion:

1.1 Sample collection and preparation: Three colonies of the Hawaiian gold coral, *Kulamanamana haumeaae* (*31*), were collected from the upper mesopelagic zone of the Hawaiian archipelago (water depths 400-450m) using the HURL/NOAA Pisces V submersible (*7*). Specimens Ger9701 and Ger9702 were collected at Makapuu Bank, off Oahu, in 1997 and were live and dead respectively. PV694 from French Frigate shoals was live-collected in 2007 (Fig. 1). Colonies were rinsed with first salt and then fresh water, air-dried, sectioned, and polished according to Sherwood et al. (*8*). Sections were subsampled parallel to growth bands along radial transects from the outer edge to the center of each section using a computerized Merchantek micromill. The radial (skeleton) growth rate of *K. haumeaae* averages ~35 μm/yr (*7*). We sampled at approximately 100 μm intervals along the cross-section transect, resulting in ~3 year temporal integration for bulk $\delta^{13}C$ values. For AA $\delta^{13}C$ analyses, which have larger sample mass demands, we pooled several adjacent samples, thereby increasing the integration time reflected in our community export reconstruction (~3 to 12 year temporal integration).

The proteinaceous skeletons of deep-sea corals serve as excellent bioarchives of sinking particulate organic matter (POM), providing faithful records of the biogeochemical and stable isotope signals of newly exported production (*7, 8, 15, 32*). Extensive previous literature has shown that gorgonian, fan, and octocorals are opportunistic feeders with minimal selective

feeding bias (*33-35*). Amino acid $\delta^{13}C$ and $\delta^{15}N$ patterns as well as radiocarbon isotope analyses of live polyps and the outermost portions of the proteinaceous skeletons indicate all clearly establish newly exported surface algal production, not resuspended material, as the dominant food source for deep-sea coral (*8, 14, 36*). For these reasons, deep-sea corals have been referred to as "living sediment traps." Furthermore, the organic skeleton of deep-sea proteinaceous corals is made of an extremely durable, cross-linked, fibrillar protein that is remarkably resistant to diagenesis (*37*). Comparisons of amino acid $\delta^{15}N$ patterns (the most susceptible to degradation) on deep-sea corals up to millennial time scales show no evidence of any alteration of CSIA patterns by diagenesis or degradation at the molecular-isotopic level (*8, 36*).

1.2 Radiocarbon dating and age models: Details of the radiocarbon dating and age models can be found in the supplemental information of Sherwood et al. (*8*). Briefly, radiocarbon dating was performed on 8 to 10 sample aliquots from each section of *K. haumeaae* at the Center for Accelerator Mass Spectrometry (CAMS), Lawrence Livermore National Laboratory. Calibrated years before present ages and age models were generated with Clam version 2.0 (*38*) and a local reservoir (ΔR) correction (*39*) of -34 ± 13 years using the Marine09 database (*40*). In general, calendar age uncertainties for the model are several decades or more. The underlying ^{14}C-calendar year calibration data for the interval spanned by our corals is the same as that in IntCal 13 (*41*).

1.3 Bulk C isotope analysis: $\delta^{13}C$ values, defined as $\delta^{13}C_{sample} = [(^{13}C/^{12}C_{sample} - {}^{13}C/^{12}C_{standard})/ {}^{13}C/^{12}C_{standard}]*1000$ were measured on 0.3 mg aliquots of all samples using a Carlo Erba 1108 elemental analyzer interfaced to a Thermo Finningan Delta Plus XP isotope ratio mass spectrometer (IRMS) at the Stable Isotope Lab, University of California, Santa Cruz. Raw isotope values were corrected for instrument drift and linearity effects, calibrated against the in

house isotopic reference materials of the Stable Isotope lab (http://emerald.ucsc.edu/~silab/), and reported in per mil (‰) relative to Vienna PeeDee Belemnite. Reproducibility, as measured by two lab standards, averaged 0.05‰.

1.4 Amino acid stable isotope analysis: Sample composites (combining 1 to 4 separate samples to obtain a total mass of 3-5 mg) were hydrolysed in 1 ml of 6N HCl at 110°C for 20 h and spiked with a norleucine internal standard. The hydrolysates were evaporated to dryness under a gentle stream of N_2 and then immediately derivatized by esterification with acidified iso-propanol followed by acylation with trifluoroacetic anhydride (*42*). For amino acid (AA) $\delta^{13}C$ analyses, the derivatized AAs were brought up in dichloromethane (DCM) and injected on column in split mode at 250°C and separated on a DB-5 column (50 m x 0.5 mm inner diameter; 0.25 μm film thickness; Agilent Technologies, Santa Clara, California, USA) in a Thermo Trace Ultra gas chromatograph (GC) at the University of California, Santa Cruz. The separated AA peaks were analyzed on a Finnegan MAT Delta^{Plus} XL IRMS interfaced to the GC through a GC-C III combustion furnace (960°C) and reduction furnace (630°C). Standardization of runs was achieved using intermittent pulses of a CO_2 reference gas of known isotopic value. Mean $\delta^{13}C$ reproducibility, as measured by a lab cyanobacteria standard, was ± 0.66‰ averaged across all individual AAs, and ± 0.35‰ averaged across essential AAs.

1.5 Individual amino acid composition and $\delta^{13}C$ values and Suess Effect corrections: We analyzed the $\delta^{13}C$ values of eleven individual AAs (table S1, S2) using the protocol of McMahon et al. (*42*), which accounted for 86 molar percent of the total hydrolysable AAs in this species' skeletal protein (*8*). Note that the molar composition estimate does not account for arginine (Arg), cysteine (Cys), and histidine (His), which cannot be determined using our methodology owing to their breakdown during acid hydrolysis. The essential AA histidine, in particular, may

represent a significant proportion of the total amino acids in gorgonin protein (*43*).

Based on established classifications (*14*), we assigned glutamic acid (Glu), aspartic acid (Asp), alanine (Ala), proline (Pro), glycine (Gly), and serine (Ser) as non-essential AAs, and threonine (Thr), leucine (Leu), isoleucine (Ile), valine (Val), and phenylalanine (Phe) as essential AAs. Acid hydrolysis converts glutamine (Gln) and aspartamine (Asn) into Glu and Asp, respectively, due to cleavage of the terminal amine group, resulting in the measurement of combined Gln + Glu (referred to hereby as Glu), and Asn +Asp (referred to hereby as Asp). While some researchers refer to these groupings as Glx and Asx, we chose our terminology here to be consistent with most CSIA studies.

For all further analyses, we used $\delta^{13}C$ data corrected for the Suess Effect using an ice-core–based estimate of the rate of $\delta^{13}C$ decrease in the atmosphere: 0.16‰ per decade since 1960, and 0.05‰ per decade between 1860 and 1960 (*9, 10*). The largest correction, approximately 1.0‰ for the most recent time point (1992) in our data set, explained approximately half of the total range in bulk $\delta^{13}C$ value (1.8‰) between the present minimum and the historic maximum in the late 1800s. However, the Suess Effect explained only a small fraction of the variability in essential AA $\delta^{13}C$ values ($\delta^{13}C_{EAA}$) (mean range between maximum and minimum $\delta^{13}C_{EAA}$ = 6.5 ± 2‰). More importantly, because $\delta^{13}C_{EAA}$ values are always normalized to the mean for $\delta^{13}C_{EAA}$ fingerprinting, as discussed below, the Suess correction is irrelevant to isotopic fingerprints of the source end-members, and thus cannot affect the Bayesian mixing model results or the subsequent conclusions.

We examined the relationship between $\delta^{13}C_{bulk}$ and individual $\delta^{13}C_{AA}$ values via reduced major axis regression (Fig. S1). We performed for the ordinary least square regressions a global validation of linear model assumptions as well separate evaluations of skewness, kurtosis, and

heteroscedasticity. The model assumptions were accepted for all fits and all models were highly significant ($p < 0.01$). We found strong positive relationships between most essential $\delta^{13}C_{AA}$ and $\delta^{13}C_{bulk}$ values indicating that most of the variability in $\delta^{13}C_{bulk}$ can be attributed to changes in source carbon at the base of the food web. We caution, however, about extrapolation of this observation to other proteinaceous deep-sea corals. Depending on the relative composition of essential versus non-essential amino acids, the relationship between bulk $\delta^{13}C$ and $\delta^{13}C_{EAA}$ may not be the same (*15*).

1.6 Compound-specific isotopic fingerprinting: In order to constrain past changes in plankton community composition contributing to export production in the North Pacific Subtropical Gyre (NPSG), we have developed new biomarkers of plankton identity based upon a powerful AA isotope fingerprinting approach (*13, 44*). We characterized unique AA isotope fingerprints for four source end-members, eukaryotic microalgae, N_2-fixing cyanobacteria, non-N_2-fixing cyanobacteria, and heterotrophic bacteria, that are key contributors to the carbon exported to the mesopelagic zone in the NPSG (*2*). The source end-members were based on a subset of molecular-isotopic training data sets from Lehman (*45*) (culture conditions presented in McCarthy et al. *46*) and Larsen et al. (*13, 44*) (table S2).

We targeted only the environmentally relevant marine end-members in both previously published training data sets and did not include terrestrial plants, marine macroalgae, or fungi samples that were used in earlier work. We also focused our analyses on only essential AAs (threonine, valine, isoleucine, phenylalanine, and leucine). The $\delta^{13}C_{EAA}$ patterns represent the sum of the isotopic fractionations associated with individual biosynthetic pathways and associated branch points for each EAA (*12, 47*), generating phylogenetically diagnostic AA fingerprints of source end-member origin (*13, 44*). Because essential AAs have very long and

complex biosynthetic pathways (five or more synthetic steps), the $\delta^{13}C_{EAA}$ are expected to provide great potential for lineage-specific isotope effects (*48, 49*). A second key aspect of using EAAs is the fact that $\delta^{13}C_{EAA}$ patterns of source end-members are preserved, essentially unchanged, across trophic transfers (*14, 42*), which has been verified in deep-sea corals (*15*). This is because, while plants, algae, and bacteria can synthesize essential amino acids *de novo,* metazoans have lost the necessary enzymatic capabilities and must acquire essential AAs directly from their diet with minimal fractionation (*50*). By focusing on the $\delta^{13}C_{EAA}$ values of source end-members relevant to the NPSG, we were thus able to achieve much better separation of our four target source end-members in $\delta^{13}C_{EAA}$ multivariate space than was originally achieved by Larsen et al. (*13*).

In order to compare the essential AA fingerprints of our four source end-member groups and corals through time, we examined $\delta^{13}C_{EAA}$ values normalized to the mean of all five essential AAs for each sample. All four source end-members were clearly separated in multivariate PCA space (Fig. S2) with within-group variability far smaller than among group variability despite samples coming from laboratory and field collections across a range of environmental gradients. As expected, there is strong experimental and field-based evidence that primary producer $\delta^{13}C_{EAA}$ fingerprints are faithful and robust across large environmental gradients in growing conditions and carbon sources that can affect bulk $\delta^{13}C$ values (*13, 16*). This is because the underlying biochemical mechanisms generating unique internally normalized $\delta^{13}C_{EAA}$ fingerprints are driven by major evolutionary diversity in the central synthesis and metabolism of AAs. For example, Larsen et al. (*13*) examined the extent to which normalized $\delta^{13}C_{EAA}$ fingerprints were affected by environmental conditions by looking at seagrass (*Posidonia oceanica*) and giant kelp communities (*Macrocystis pyrifera*) across a variety of oceanographic

and growth conditions (see Larsen et al. *13* Table S1 for details). For both species, the range in bulk $\delta^{13}C$ values was five- to ten-times greater (2.6‰ and 5.2‰, respectively) than it was for normalized $\delta^{13}C_{EAA}$ values (0.4‰ to 0.6‰, respectively). By normalizing the individual $\delta^{13}C_{EAA}$ values to the mean, Larsen et al. (*13*) showed that natural variability in $\delta^{13}C$ values of individual amino acids is effectively removed, creating diagnostic fingerprints that were independent of environmental conditions. Larsen et al. (*16*) also conducted the first directly controlled physiological studies of normalized $\delta^{13}C_{EAA}$ fingerprint fidelity using a laboratory-cultured marine diatom, *Thalassiosira weissflogii*, grown under a wide range of conditions: light, salinity, temperature, and pH. This study showed that normalized $\delta^{13}C_{EAA}$ values remained essentially unmodified despite very large changes in bulk and raw amino acid $\delta^{13}C$ values (>10‰), molar percent abundances of individual amino acids, and total cellular carbon to nitrogen ratios. Together, Larsen et al. (*13, 16*) provide strong evidence that normalized EAA $\delta^{13}C$ fingerprints are diagnostic of the primary producer source rather than the myriad factors affecting bulk $\delta^{13}C$ values such as carbon availability, growth conditions, and oceanographic conditions. Finally, Schiff et al. (*15*) confirmed this conclusion for deep-sea corals by showing excellent agreement between the normalized $\delta^{13}C_{EAA}$ fingerprints of deep-sea bamboo coral, *Isidella sp.*, from Monterey Canyon and field-collected eukaryotic microalgae from the California coast (*51*). As such, we are confident that the normalized $\delta^{13}C_{EAA}$ fingerprints of laboratory-cultured and field-collected source end-members are robust, faithful proxies of the identity of major carbon sources for deep-sea corals, regardless of the exact location and growing conditions of the end-members.

We present the multivariate signatures of $\delta^{13}C_{EAA}$ values from source end-members and coral samples using principal component analysis (PCA) of the covariance matrix. We found significant separation in essential AA $\delta^{13}C$ patterns of Thr, Ile, Phe, and Leu, among the four

major sources of carbon in sinking POM being exported to the mesopelagic zone (Fig. S2a): three photoautrophic algal groups (non-N_2 fixing cyanobacteria, N_2-fixing cyanobacteria, eukaryotic microalgae) and heterotrophic bacteria that remineralize sinking POM. The first two principal components explained 78% of the total variation in the model (Fig. S2b). Along the first principal component, Thr (-0.67) and Leu (0.57) were particularly powerful separators, while Phe (-0.60) and Ile (0.61) showed the greatest separation power along principal component 2 (Fig. S2b).

1.7 Bayesian stable isotope mixing model and hierarchical clustering analysis: We estimated the relative contributions of carbon from the four source end-members (non-N_2 fixing cyanobacteria, N_2-fixing cyanobacteria, eukaryotic microalgae, and heterotrophic bacteria) to *K. haumeaae* using a fully Bayesian approach (*52, 53*) within the Stable Isotope Analysis in R (SIAR) package (*54*). Four essential AAs (Thr, Ile, Phe, and Leu) were used in the mixing model, which showed the greatest separation power, to conform to model specifications. In SIAR, we ran 500,000 iterations with an initial discard of the first 50,000 iterations as burn-in. By using $\delta^{13}C_{EAA}$ values within the Bayesian isotope mixing model, we avoid the major issue that plagues poorly resolved dual isotope approaches in multi-end-member systems (*55, 56*): underdetermined mixing, and complications of variable and poorly characterized trophic fractionation (*57*). Galloway et al. (*58, 59*) demonstrated great success using a similar approach with fatty acid profiles and Bayesian mixing models to examine resource utilization in zooplankton and isopods. However, AAs are particularly valuable tracers of carbon flow because they are major biochemical constituents of all organic matter, accounting for approximately half of the total organic carbon (and most of the organic nitrogen) in organisms (*60*).

As noted in the main text, our results clearly show a pronounced increase in the relative

185 contribution of N_2-fixing cyanobacteria over the past 100 years with a concurrent decrease in the
186 relative contribution of eukaryotic microalgae. While the exact $\delta^{13}C_{EAA}$ fingerprints of the
187 common N_2-fixing cyanobacteria/diatom symbioses in the NPSG (e.g. the cyanobacteria *Richelia*
188 *sp.* and the diatom e.g. *Rhizosolenia sp.*; e.g. *22*) have never been directly tested, the contrast in
189 eukaryotic versus N_2-fixing cyanobacteria contributions to export production over time suggests
190 that the increase in the N_2-fixation signal since the LIA has largely been derived from free-living
191 cyanobacteria. Karl et al. (*22*) recently suggested that pronounced summertime export pulses of
192 sinking POM to the deep ocean in the NPSG are primarily caused by increases in the biomass
193 and productivity of symbiotic nitrogen-fixing cyanobacteria in association with diatoms. The
194 temporal resolution of our long0term coral data set (~20-years) is not sufficient to resolve such
195 fine scale, seasonal shifts in export production, and thus our conclusions are correspondingly
196 focused on much longer term centennial scale shifts in export production. Regardless, any
197 uncertainty about the exact nature of the phylogenetic identity of the source of increasing N_2-
198 fixation does not affect our central conclusions that the end of the Little Ice Age and the start of
199 the Industrial Era have brought with them a fundamental shift towards increased contribution of
200 N_2-fixing cyanobacteria to carbon being exported to the mesopelagic zone.

201 We saw no long-term secular trend in heterotrophic bacterial carbon contribution during
202 the past 1000 year trend ($f(x) = 0.0x-0.1$, $r^2 = 0.60$), suggesting that changes in the degree of
203 heterotrophic microbial reworking of sinking POM did not significantly contribute to the patterns
204 of change in $\delta^{13}C_{bulk}$ (Fig. 2a). This conclusion was independently supported by stable nitrogen
205 isotope analyses of individual AAs from these same corals (*9*), which showed no long-term trend
206 in ΣV, a measure of variance in $\delta^{15}N_{AA}$ associated with microbial resynthesis of AAs [see
207 Extended Data Fig. 3 in Sherwood et al. (*8*)]. However, these conclusions only refer to the

208 contribution of AAs from heterotrophic bacteria as a proxy for the degree of microbial reworking
209 exported POM. Our training dataset did not allow us to distinguish among taxonomic groups
210 within the heterotrophic bacteria end-member, and thus our data cannot address the possibility of
211 systematic changes in the taxonomic composition of heterotrophic bacteria through time. Finally,
212 it should be noted that the corals used in this study were collected in the upper NPSG
213 mesopelagic zone (~450m), where substantial degradation of sinking POM should already have
214 occurred (*61*). If cyanobacterial primary production were remineralized at different rates relative
215 to eukaryotic material, this could also represent an additional mechanism influencing its relative
216 importance as a proportion of carbon export to the ocean's interior. However, to our knowledge
217 there is no evidence for this in the literature, nor any organic geochemical expectation that it
218 might occur. Furthermore, any such systematic offsets in transfer to depth based on algal group
219 should apply throughout our record.

220 The Bayesian mixing model results from deep-sea coral $\delta^{13}C_{EAA}$ values provided
221 quantitative evidence of fundamental shifts in the phylogenetic identity of past phytoplankton
222 assemblages contributing to exported production in the NPSG, likely linked to multicentennial
223 scale changes in climate and oceanographic condition. While our study directly examined
224 changes in the phylogenetic identity of exported production and not the actual surface ocean
225 plankton community composition, it would seem extraordinarily unlikely that changes the former
226 could occur in isolation from the latter. Thus the most parsimonious explanation of our data is
227 that the observed changes in the source of carbon to export production reflect changes in the
228 surface plankton community composition. An alternative hypothesis is that surface plankton
229 community composition has remained relatively constant through time, and instead the degree of
230 decoupling between surface and export production has undergone dramatic changes as a function

of climate shifts. While our data cannot directly rule out this alternative hypothesis, this idea seems highly unlikely. To our knowledge there is also no proposed mechanism in the literature that would support such a dramatic change in coupling, and no organic geochemical basis for dramatic shifts in relative degradation of different fresh algal sources.

To better constrain the pattern of changing plankton community composition, we applied hierarchical cluster analysis to the CSIA data to reveal time periods of similar primary carbon export sources. Hierarchical clustering analysis of the plankton carbon utilization data was performed in R (*54*). Bootstrap probabilities of the resulting dendrogram were calculated using the "pvclust" package in R (10,000 replications). Clusters with multiscale bootstrap (approximately unbiased) p values > 0.95 were considered strongly supported and statistically significant ($\alpha = 0.05$). This process resulted in a well-ordered dendrogram that identified three clusters of significantly different plankton carbon contribution with strong temporal continuity. The first temporal cluster was characterized by strong non-N_2 fixing cyanobacterial production and comprised the years 1036C.E. to 1564C.E. The second temporal cluster was characterized by enhanced eukaryotic microalgal production and encompassed the years 1595C.E. to 1875C.E. The third cluster was characterized by enhanced N_2-fixing cyanobacterial production and included the years 1934C.E. to the present.

1.8 Independence of $\delta^{13}C$ and $\delta^{15}N$ fractionation of amino acids: As noted in the main text, our results suggest that the rapid climate transition at the end of the Little Ice Age and the onset of the industrial revolution coincided with a shift in NPSG plankton community composition unprecedented in the last 1000 years, to a system with export production dominated by N_2-fixing cyanobacteria. Sherwood et al. (*8*) provided independent evidence for a concurrent increase in N_2-fixation since the end of the Little Ice Age. These authors used AA $\delta^{15}N$ analyses of the same

254 deep-sea corals as our current study to show that the dramatic decrease in sinking POM $\delta^{15}N$
255 values around Hawaii since the 1800s most likely represented a ca. 30% increase in N_2-fixation
256 in the region.

257 An important element of these data sets is the understanding that records derived from
258 $d^{15}N$ and $d^{13}C$ data within AA molecules are effectively fully independent. The results from
259 Sherwood et al. (*8*) are based on the fact that $\delta^{15}N$ values of amino acids (i.e., the $\delta^{15}N$ value of
260 the amine N atom for most AAs) display distinct fractionation patterns during trophic transfer.
261 These differences in fractionation form the basis for dividing AAs into two groups (*62*): the
262 trophic AAs (showing large fractionation with trophic transfer) and the source AAs (showing
263 minimal fractionation with trophic transfer). Amino acid nitrogen isotope fractionation is driven
264 primarily by fractionation of the amide N atom linked to the constant balance of
265 transamination/deamination relative to the central N pool of a cell during amino acid metabolism
266 (*63, 64*). The canonical source AA, phenylalanine (Phe), shows minimal trophic fractionation in
267 its amide N between diet and consumer, because its metabolic processing does not form or break
268 the amide C-N bond (*63-65*). Thus Phe $\delta^{15}N$ values provide a direct proxy for the $\delta^{15}N$ signatures
269 of the nitrogen sources at the base of the food web that get passed on to upper trophic level
270 consumers virtually unmodified (*8, 66*).

271 The processes for $\delta^{15}N$ fractionation, based on amide $\delta^{15}N$ value and
272 transamination/deamination balance, are completely independent from the processes controlling
273 AA carbon isotope fractionation. Carbon isotope fractionation in AAs is linked to the enzymatic
274 pathways for the biosynthesis of of the carbon skeleton (primarily the side chain) of each AA
275 (*14, 42*). While all consumers can synthesize non-essential AAs from a bulk carbon pool,
276 animals have lost the enzymatic ability to synthesize essential AAs at a rate sufficient for normal

277 growth and must acquire them from their diet (*50*). The $\delta^{13}C_{EAA}$ of animals is therefore fixed by
278 the $\delta^{13}C_{EAA}$ of primary producers at the base of the food web. As discussed above, the metabolic
279 diversity of essential AA synthesis pathways, including the enzymatic steps and associated
280 isotope effects (*12, 47*), creates unique isotopic fingerprints of primary producers groups that are
281 passed on to upper trophic level consumers virtually unmodified (*13, 15, 44, 51, 67, 68*). As a
282 result, the degree of carbon isotope fractionation for essential AAs (virtually 0‰ for animals) is
283 completely decoupled from the fractionation of N in source amino acids. Therefore, $\delta^{13}C_{EAA}$
284 provides a robust tracer of the primary producer sources of carbon to a food web, independent of
285 the sources and cycling of N at the base of the food web recorded in source $\delta^{15}N$ values.
286
287
288
289
290
291
292
293
294
295
296
297
298
299

2.0 Supplementary Figures:

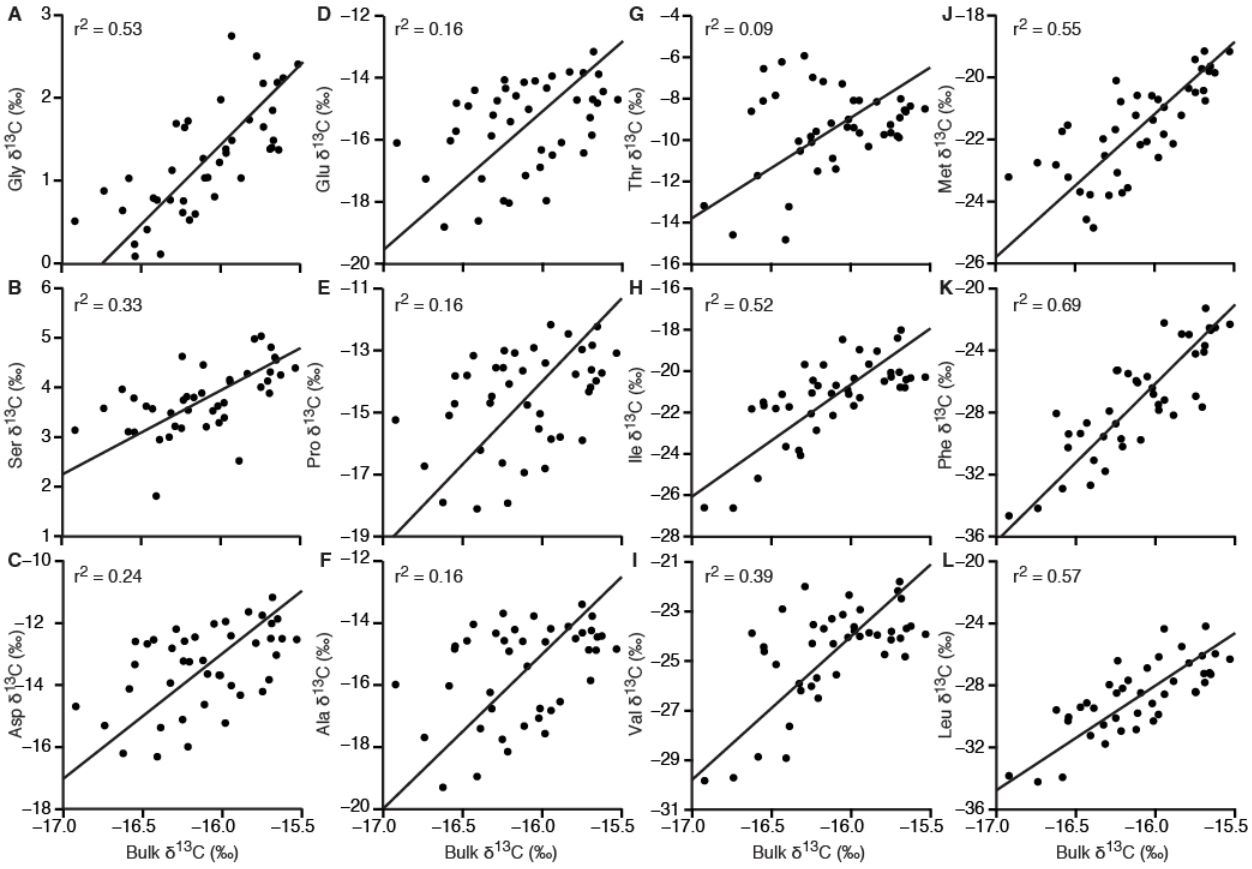

Figure S1. Linear regressions of amino acid and bulk $\delta^{13}C$ values

Reduced major axis regression of bulk and individual amino acid $\delta^{13}C$ values for deep-sea corals collected from Makapuu and French Frigate Shoals in the North Pacific Subtropical Gyre. Panels **A-F** are non-essential amino acids: glycine (Gly), serine (Ser), aspartic acid (Asp), glutamic acid (Glu), proline (Pro), alanine (Ala), and panels **G-L** are essential amino acids: threonine (Thr), isoleucine (Ile), valine (Val), methionine (Met), phenylalanine (Phe), and leucine (Leu). We found for all fits that the model assumptions were accepted and all models were highly significant ($p < 0.01$).

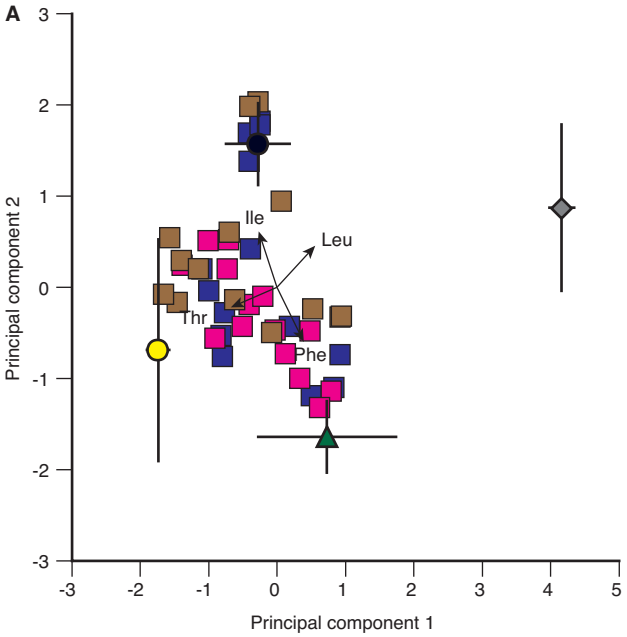

	PC1	PC2	PC3	PC4
Threonine^{E}	-0.67	-0.21	0.24	0.67
Isoleucine^{E}	-0.26	0.61	-0.72	0.19
Phenylalanine^{E}	0.41	-0.60	-0.55	0.41
Leucine^{E}	0.57	0.47	0.34	0.58
Variance	0.50	0.28	0.21	0.01

Figure S2. Principal component analysis of deep-sea coral and source end-member $\delta^{13}C$ values.

A) Principal component analysis of phytoplankton and coral essential amino acid $\delta^{13}C$. Separation of plankton end-members (nitrogen fixing cyanobacteria black circle; non-nitrogen fixing cyanobacteria yellow circle; eukaryotic microalgae green triangle; heterotrophic bacteria gray diamond) and *K. haumeaae* (open squares following color scheme in Fig. S1) in principal component space based on normalized essential amino acid $\delta^{13}C$ values. **B**) PCA loadings (indicated in panel **A** as arrows from the center) and variance from the principal component analysis of normalized essential amino acid $\delta^{13}C$ values from deep-sea corals and plankton source end-members.

2.0 Supplementary Tables:

Table S1. Bulk and individual amino acid $\delta^{13}C$ values of deep-sea corals.

$\delta^{13}C$ values of bulk proteinaceous skeleton and individual amino acids from deep-sea corals collected off Oahu and French Frigate Shoals in the North Pacific Subtropical Gyre. Values in this table have not been corrected for the Suess Effect. Ger9701 and Ger9702 were collected alive and dead respectively in 1997 from Makapuu off Oahu, and FFS694 was collected alive from French Frigate Shoals in 2007. Essential amino acids designated with ^{E}. Abbreviations according to Fig. 1S.

Coral ID	Year	Bulk	Gly	Ser	Asp	Glu	Pro	Ala	Thr^{E}	Met^{E}	Ile^{E}	Val^{E}	Phe^{E}	Leu^{E}
GER9701	1968	-17.0	0.1	1.2	-16.9	-19.3	-18.7	-19.6	-15.5	-24.4	-24.3	-29.5	-33.3	-31.9
GER9701	1951	-16.6	0.6	2.8	-14.1	-15.5	-15.2	-15.9	-11.9	-22.6	-21.1	-26.0	-30.2	-28.9
GER9701	1942	-16.3	0.6	2.1	-14.7	-16.5	-16.2	-16.9	-10.7	-22.6	-20.1	-24.3	-28.6	-28.1
GER9701	1934	-16.1	1.0	3.8	-14.2	-15.7	-14.7	-15.2	-10.2	-20.1	-18.8	-22.5	-28.0	-26.5
GER9701	1886	-15.9	1.5	4.9	-14.3	-16.6	-16.0	-14.4	-9.8	-20.6	-20.4	-23.9	-27.1	-28.6
GER9701	1827	-15.7	1.4	4.6	-11.9	-13.9	-12.2	-14.5	-8.6	-19.6	-20.4	-23.7	-22.7	-27.3
GER9701	1724	-15.6	2.2	4.3	-12.5	-14.4	-13.7	-14.4	-8.4	-19.9	-20.3	-23.6	-22.5	-26.0
GER9701	1647	-15.8	2.5	5.0	-12.7	-14.7	-13.8	-14.5	-9.7	-20.4	-20.5	-24.7	-23.0	-26.6
GER9701	1595	-16.3	0.8	4.6	-13.2	-14.1	-13.6	-13.7	-10.1	-20.1	-21.1	-24.3	-25.3	-28.5
GER9701	1489	-16.0	2.0	3.3	-13.7	-16.3	-15.0	-16.8	-9.0	-21.4	-21.1	-22.3	-26.8	-30.3
GER9701	1426	-16.1	1.3	3.9	-13.2	-14.2	-13.7	-14.6	-9.2	-21.2	-21.1	-23.3	-26.0	-30.8
GER9701	1346	-16.6	0.6	4.0	-16.2	-18.8	-17.9	-19.3	-8.6	-22.8	-21.8	-23.9	-28.1	-29.6
GER9701	1306	-16.2	1.7	3.8	-16.0	-18.0	-17.9	-18.2	-9.6	-20.8	-22.9	-25.7	-29.7	-30.9
GER9701	1249	-16.3	1.1	3.5	-12.8	-15.2	-14.5	-16.8	-10.5	-22.5	-24.1	-26.2	-31.8	-31.8
GER9702	1781	-15.8	2.2	4.0	-11.8	-13.8	-13.0	-13.4	-9.3	-19.4	-20.1	-24.1	-24.2	-28.4
GER9702	1752	-15.7	1.9	4.3	-12.0	-14.7	-13.6	-14.2	-8.9	-19.2	-20.8	-24.1	-23.7	-27.8
GER9702	1722	-15.5	2.4	4.4	-12.5	-14.7	-13.1	-14.8	-8.5	-19.2	-20.3	-23.9	-22.3	-26.3
GER9702	1684	-15.7	2.2	4.6	-13.0	-14.8	-14.0	-14.9	-8.6	-19.8	-20.8	-24.8	-22.5	-27.2
GER9702	1628	-15.7	1.4	3.9	-12.5	-15.9	-14.2	-15.9	-9.9	-20.4	-20.1	-21.8	-24.1	-27.2
GER9702	1564	-16.0	1.2	3.6	-13.7	-16.9	-15.5	-17.1	-9.4	-20.6	-20.9	-24.1	-26.4	-29.2

GER9702	1512	-15.9	1.5	4.1	-14.0	-16.5	-15.9	-16.8	-9.7	-21.0	-21.3	-22.9	-27.2	-28.6
GER9702	1453	-16.1	1.0	4.5	-14.6	-17.2	-16.9	-17.3	-10.9	-20.6	-22.1	-24.3	-26.1	-29.8
GER9702	1368	-16.0	1.4	3.7	-15.2	-18.0	-16.8	-17.6	-8.1	-20.7	-21.7	-23.6	-27.5	-29.9
GER9702	1352	-16.3	0.6	3.2	-15.1	-18.0	-16.6	-17.8	-9.8	-21.7	-22.1	-26.0	-28.7	-30.1
GER9702	1297	-16.3	0.8	3.0	-13.9	-15.9	-14.7	-16.2	-10.1	-22.0	-23.8	-25.9	-29.6	-30.5
GER9702	1233	-16.6	1.0	3.1	-14.1	-16.0	-15.1	-16.0	-11.7	-21.7	-25.2	-28.9	-32.9	-33.9
GER9702	1179	-16.9	0.5	3.1	-14.7	-16.1	-15.2	-16.0	-13.2	-23.2	-26.6	-29.8	-34.7	-33.8
GER9702	1151	-16.7	0.9	3.6	-15.3	-17.3	-16.7	-17.7	-14.6	-22.8	-26.6	-29.7	-34.2	-34.2
FFS694	1992	-17.4	-0.9	1.9	-16.4	-18.3	-17.2	-18.4	-14.2	-25.9	-22.7	-28.6	-32.1	-30.5
FFS694	1975	-17.0	-0.2	2.8	-14.0	-16.2	-14.8	-15.7	-12.3	-24.5	-21.4	-27.2	-30.9	-28.9
FFS694	1939	-16.4	0.9	3.0	-12.3	-14.7	-13.8	-15.0	-9.8	-23.0	-20.8	-24.2	-28.2	-26.6
FFS694	1875	-15.9	1.7	4.2	-11.7	-13.9	-12.5	-14.2	-8.2	-21.3	-19.1	-24.0	-23.0	-25.6
FFS694	1787	-15.7	1.5	4.8	-11.2	-13.2	-12.8	-13.8	-8.0	-20.8	-18.0	-22.5	-21.3	-24.2
FFS694	1621	-16.0	2.8	4.2	-12.4	-14.0	-12.2	-14.2	-8.1	-21.8	-19.0	-24.0	-22.2	-24.4
FFS694	1536	-16.2	1.6	3.7	-12.6	-14.3	-13.0	-14.6	-7.0	-23.1	-20.5	-23.5	-25.3	-26.4
FFS694	1448	-16.3	1.7	3.2	-12.2	-14.7	-13.6	-14.3	-5.9	-23.8	-19.7	-22.0	-27.9	-28.0
FFS694	1414	-16.1	0.8	3.5	-12.0	-14.1	-12.9	-13.8	-7.3	-22.1	-18.5	-23.1	-25.7	-26.9
FFS694	1399	-16.2	0.6	3.8	-12.5	-14.6	-13.1	-14.2	-7.2	-23.6	-19.7	-23.7	-25.5	-27.7
FFS694	1389	-16.4	0.8	3.6	-12.5	-14.4	-13.2	-14.0	-6.2	-24.6	-21.1	-22.9	-28.7	-29.1
FFS694	1340	-16.6	0.2	3.8	-13.3	-15.7	-14.7	-14.8	-8.1	-21.5	-21.5	-24.4	-30.3	-30.3
FFS694	1238	-16.5	0.4	3.6	-12.7	-14.9	-13.8	-14.6	-7.9	-23.7	-21.8	-25.1	-29.4	-29.4
FFS694	1037	-16.6	0.1	3.1	-12.6	-14.8	-13.8	-14.7	-6.6	-23.2	-21.7	-24.6	-29.4	-30.1

Table S2. Amino acid $\delta^{13}C$ values of source end-members.

$\delta^{13}C$ values of source end-members that used as the molecular-isotopic training data set (data from *13, 44, 45*). $\delta^{13}C$ values of essential amino acids were corrected for the Suess effect (*9, 10*) in the same manner as the deep-sea coral samples and then normalized to their mean. The four source end-members (N_2 fixing cyanobacteria, non N_2-fixing cyanobacteria, eukaryotic microalgae and heterotrophic bacteria) were analyzed in triplicate (mean ± SD).

Group	Latin name	Phylogeny	threonine	isoleucine	valine	phenylalanine	leucine
N_2 fixing	*Anabaena cylindrica*[13]	Cyanobacterium	12.7 ± 1.0	1.3 ± 0.1	-1.9 ± 0.2	-7.4 ± 0.1	-4.7 ± 0.3
N_2 fixing	*Nostoc muscorum*[13]	Cyanobacterium	11.5 ± 0.1	1.6 ± 0.1	-2.6 ± 0.1	-6.4 ± 0.2	-4.2 ± 0.0
N_2 fixing	*Cyanothece sp*[45]	Cyanobacterium	11.0 ± 0.2	3.7 ± 0.1	-2.6 ± 0.2	-59 ± 0.3	-6.4 ± 0.2
N_2 fixing	*Trichodesmium sp.*[45]	Cyanobacterium	11.9 ± 0.1	2.1 ± 0.2	-2.4 ± 0.2	-6.4 ± 0.2	.-5.0 ± 0.1
Non N_2 fixing	*Prochlorococcus sp.*[45]	Cyanobacterium	17.3 ± 0.3	-0.3 ± 0.1	-2.8 ± 0.1	-7.2 ± 0.1	-6.9 ± 0.2
Non N_2 fixing	*Synechococcus sp.*[45]	Cyanobacterium	16.5 ± 0.2	0.7 ± 0.1	-1.4 ± 0.2	-8.9 ± 0.2	-6.8 ± 0.1
Non N_2 fixing	*Merismopedia punctata*[13]	Cyanobacterium	17.9 ± 0.6	-1.5 ± 0.0	-1.4 ± 0.1	-6.5 ± 0.1	-8.6 ± 0.0
Euk microalgae	*Dunaliella sp.*[13]	Chlorophyte	9.8 ± 0.5	0.7 ± 1.3	-2.7 ± 0.5	-0.4 ± 0.1	-7.2 ± 0.3
Euk microalgae	*Prasinocladus marinus*[13]	Chlorophyte	13.2 ± 0.8	0.1 ± 0.5	-5.2 ± 0.1	-0.1 ± 0.0	-7.9 ± 0.1
Euk microalgae	*Melosira varians*[13]	Diatom	9.1 ± 0.9	-0.4 ± 0.1	-3.6 ± 0.2	1.1 ± 0.2	-6.0 ± 0.0
Euk microalgae	*Emiliana huxleyi*[13]	Haptophyte	10.4 ± 0.1	1.2 ± 0.6	-5.4 ± 0.0	1.6 ± 0.0	-7.7 ± 0.0
Euk microalgae	*Isochrysis galbana*[13]	Haptophyte	12.2 ± 0.2	2.8 ± 0.1	-5.7 ± 0.1	1.2 ± 0.0	-10.3 ± 0.1
Het bacteria	*Rhodococcus spp.*[44]	Actinobacteria	5.3 ± 0.1	-1.2 ± 0.1	-0.7 ± 0.2	-3.1 ± 0.1	-0.1 ± 0.2
Het bacteria	*Actinobacteria*[44]	Actinobacteria	5.9 ± 0.4	-1.5 ± 0.2	-1.3 ± 0.1	-3.0 ± 0.1	0.0 ± 0.2
Het bacteria	*Burkholderia xenovorans*[44]	Betaprotobacteria	4.6 ± 0.8	0.2 ± 0.2	-1.6 ± 0.1	-4.6 ± 0.0	1.5 ± 0.1
Het bacteria	*Escherichia coli*[44]	Gammaproteobacteria	1.8 ± 0.5	1.0 ± 0.3	-0.1 ± 0.2	-2.0 ± 0.3	-0.5 ± 0.2

REFERENCES AND NOTES

1. D. M. Karl, A sea of change: Biogeochemical variability in the North Pacific subtropical gyre. *Ecosystems* **2**, 181–214 (1999). doi:10.1007/s100219900068

2. D. M. Karl, R. R. Bidigare, R. M. Letelier, Long-term changes in plankton community structure and productivity in the North Pacific Subtropical Gyre: The domain shift hypothesis. *Deep Sea Res. Part II Top. Stud. Oceanogr.* **48**, 1449–1470 (2001). doi:10.1016/S0967-0645(00)00149-1

3. T. L. Richardson, G. A. Jackson, Small phytoplankton and carbon export from the surface ocean. *Science* **315**, 838–840 (2007). Medline doi:10.1126/science.1133471

4. J. E. Dore, R. M. Letelier, M. J. Church, R. Lukas, D. M. Karl, Summer phytoplankton blooms in the oligotrophic North Pacific Subtropical Gyre: Historical perspective and recent observations. *Prog. Oceanogr.* **76**, 2–38 (2008). doi:10.1016/j.pocean.2007.10.002

5. G. C. Hays, A. J. Richardson, C. Robinson, Climate change and marine plankton. *Trends Ecol. Evol.* **20**, 337–344 (2005). Medline doi:10.1016/j.tree.2005.03.004

6. J. J. Polovina, E. A. Howell, M. Abecassis, Ocean's least productive waters are expanding. *Geophys. Res. Lett.* **35**, L03618 (2008). doi:10.1029/2007GL031745

7. T. P. Guilderson, M. D. McCarthy, R. B. Dunbar, A. Englebrecht, E. B. Roark, Late Holocene variations in Pacific surface circulation and biogeochemistry inferred from proteinaceous deep-sea corals. *Biogeosciences* **10**, 6019–6028 (2013). doi:10.5194/bg-10-6019-2013

8. O. A. Sherwood, T. P. Guilderson, F. C. Batista, J. T. Schiff, M. D. McCarthy, Increasing subtropical North Pacific Ocean nitrogen fixation since the Little Ice Age. *Nature* **505**, 78–81 (2014). Medline doi:10.1038/nature12784

9. R. J. Francey, C. E. Allison, D. M. Etheridge, C. M. Trudinger, I. G. Enting, M. Leuenberger, R. L. Langenfelds, E. Michel, L. P. Steele, A 1000-year high precision record of $\delta^{13}C$ in atmospheric CO_2. *Tellus B Chem. Phys. Meteorol.* **51**, 170–193 (1999). doi:10.1034/j.1600-0889.1999.t01-1-00005.x

10. P. Quay, R. Sonnerup, T. Westby, J Stutsman, A. McNichol. Changes in the $^{13}C/^{12}C$ of dissolved inorganic carbon in the ocean as a tracer of anthropogenic CO_2 uptake. *Global Biogeochem. Cycles* **17**, 4-1–4-20 (2013).

11. Materials and methods are available as supplementary materials on *Science* Online.

12. J. H. Scott, D. M. O'Brien, D. Emerson, H. Sun, G. D. McDonald, A. Salgado, M. L. Fogel, An examination of the carbon isotope effects associated with amino acid biosynthesis. *Astrobiology* **6**, 867–880 (2006). Medline doi:10.1089/ast.2006.6.867

13. T. Larsen, M. Ventura, N. Andersen, D. M. O'Brien, U. Piatkowski, M. D. McCarthy, Tracing carbon sources through aquatic and terrestrial food webs using amino acid stable isotope fingerprinting. *PLOS ONE* **8**, e73441 (2013). Medline doi:10.1371/journal.pone.0073441

14. K. W. McMahon, L.-L. Hamady, S. R. Thorrold, Ocean ecogeochemistry: A review. *Oceanogr. Mar. Biol. Annu. Rev.* **51**, 327–374 (2013).

15. J. T. Schiff, F. C. Batista, O. A. Sherwood, T. P. Guilderson, T. M. Hill, A. C. Ravelo, K. W. McMahon, M. D. McCarthy, Compound specific amino acid $\delta^{13}C$ patterns in a deep-sea proteinaceous coral: Implications for reconstructing detailed $\delta^{13}C$ records of exported primary production. *Mar. Chem.* **166**, 82–91 (2014). doi:10.1016/j.marchem.2014.09.008

16. T. Larsen, L. T. Bach, R. Salvatteci, Y. V. Wang, N. Andersen, M. Ventura, M. D. McCarthy, Assessing the potential of amino acid $\delta^{13}C$ patterns as a carbon source tracer in marine sediments: Effects of algal growth conditions and sedimentary diagenesis. *Biogeosciences* **12**, 4979–4992 (2015). doi:10.5194/bg-12-4979-2015

17. R. Scharek, M. Latasa, D. M. Karl, R. R. Bidigare, Temporal variations in diatom abundance and downward vertical flux in the oligotrophic North Pacific gyre. *Deep Sea Res. Part I Oceanogr. Res. Pap.* **46**, 1051–1075 (1999). doi:10.1016/S0967-0637(98)00102-2

18. M. E. Mann, Z. Zhang, S. Rutherford, R. S. Bradley, M. K. Hughes, D. Shindell, C. Ammann, G. Faluvegi, F. Ni, Global signatures and dynamical origins of the Little Ice Age and Medieval Climate Anomaly. *Science* **326**, 1256–1260 (2009). Medline doi:10.1126/science.1177303

19. V. Trouet, J. Esper, N. E. Graham, A. Baker, J. D. Scourse, D. C. Frank, Persistent positive North Atlantic oscillation mode dominated the Medieval Climate Anomaly. *Science* **324**, 78–80 (2009). Medline doi:10.1126/science.1166349

20. G. Corno, D. M. Karl, M. J. Church, R. M. Letelier, R. Lukas, R. R. Bidigare, M. R. Abbott, Impact of climate forcing on ecosystem processes in the North Pacific Subtropical Gyre. *J. Geophys. Res.* **112**, C04021 (2007). doi:10.1029/2006JC003730

21. R. W. Eppley, E. H. Renger, E. L. Venrick, M. M. Mullin, A study of plankton dynamics and nutrient cycling in the central gyre of the North Pacific Ocean. *Limnol. Oceanogr.* **18**, 534–551 (1973). doi:10.4319/lo.1973.18.4.0534

22. D. M. Karl, M. J. Church, J. E. Dore, R. M. Letelier, C. Mahaffey, Predictable and efficient carbon sequestration in the North Pacific Ocean supported by symbiotic nitrogen fixation. *Proc. Natl. Acad. Sci. U.S.A.* **109**, 1842–1849 (2012). Medline doi:10.1073/pnas.1120312109

23. A. C. Martiny, C. T. A. Pham, F. W. Primeau, J. A. Vrugt, J. K. Moore, S. A. Levin, M. W. Lomas, Strong latitudinal patterns in the elemental ratios of marine plankton and organic matter. *Nat. Geosci.* **6**, 279–283 (2013). doi:10.1038/ngeo1757

24. Y. C. Teng, F. W. Primeau, J. K. Moore, M. W. Lomas, A. C. Martiny, Global-scale variations of the ratios of carbon to phosphorus in exported marine organic matter. *Nat. Geosci.* **7**, 895–898 (2014). doi:10.1038/ngeo2303

25. C. Deutsch, W. Berelson, R. Thunell, T. Weber, C. Tems, J. McManus, J. Crusius, T. Ito, T. Baumgartner, V. Ferreira, J. Mey, A. van Geen, Centennial changes in North Pacific anoxia linked to tropical trade winds. *Science* **345**, 665–668 (2014). Medline doi:10.1126/science.1252332

26. I. N. Kim, K. Lee, N. Gruber, D. M. Karl, J. L. Bullister, S. Yang, T. W. Kim, Increasing anthropogenic nitrogen in the North Pacific Ocean. *Science* **346**, 1102–1106 (2014). Medline doi:10.1126/science.1258396

27. P. Flombaum, J. L. Gallegos, R. A. Gordillo, J. Rincón, L. L. Zabala, N. Jiao, D. M. Karl, W. K. Li, M. W. Lomas, D. Veneziano, C. S. Vera, J. A. Vrugt, A. C. Martiny, Present and future global distributions of the marine Cyanobacteria *Prochlorococcus* and *Synechococcus*. *Proc. Natl. Acad. Sci. U.S.A.* **110**, 9824–9829 (2013). Medline doi:10.1073/pnas.1307701110

28. P. G. Falkowski, R. T. Barber, V. Smetacek, Biogeochemical controls and feedbacks on ocean primary production. *Science* **281**, 200–206 (1998). Medline doi:10.1126/science.281.5374.200

29. P. W. Boyd, P. P. Newton, Does planktonic community structure determine downward particulate organic carbon flux in different oceanic provinces? *Deep Sea Res. Part I Oceanogr. Res. Pap.* **46**, 63–91 (1999). doi:10.1016/S0967-0637(98)00066-1

30. H. G. Close, S. R. Shah, A. E. Ingalls, A. F. Diefendorf, E. L. Brodie, R. L. Hansman, K. H. Freeman, L. I. Aluwihare, A. Pearson, Export of submicron particulate organic matter to mesopelagic depth in an oligotrophic gyre. *Proc. Natl. Acad. Sci. U.S.A.* **110**, 12565–12570 (2013). Medline doi:10.1073/pnas.1217514110

31. F. Sinniger, O. V. Ocaña, A. R. Baco, Diversity of zoanthids (Anthozoa: Hexacorallia) on Hawaiian seamounts: Description of the Hawaiian gold coral and additional zoanthids. *PLOS ONE* **8**, e52607 (2013). Medline doi:10.1371/journal.pone.0052607

32. E. B. Roark, T. P. Guilderson, R. B. Dunbar, S. J. Fallon, D. A. Mucciarone, Extreme longevity in proteinaceous deep-sea corals. *Proc. Natl. Acad. Sci. U.S.A.* **106**, 5204–5208 (2009). Medline doi:10.1073/pnas.0810875106

33. M. Ribes, R. Coma, J.-M. Gili, Heterogeneous feeding in benthic suspension feeders: The natural diet and grazing rate of the temperate gorgonian *Paramuricea clavata* (Cnidaria: Octocorallia) over a year cycle. *Mar. Ecol. Prog. Ser.* **183**, 125–137 (1999). doi:10.3354/meps183125

34. R. Coma, M. Ribes, J.-M. Gili, R. N. Hughes, The ultimate opportunists: Consumers of seston. *Mar. Ecol. Prog. Ser.* **219**, 305–308 (2001). doi:10.3354/meps219305

35. C. Orejas, J.-M. Gili, W. Arntz, Role of small-plankton communities in the diet of two Antarctic octocorals (*Primnoisis antarctica* and *Primnoella* sp.). *Mar. Ecol. Prog. Ser.* **250**, 105–116 (2003). doi:10.3354/meps250105

36. O. A. Sherwood, M. F. Lehmann, C. J. Schubert, D. B. Scott, M. D. McCarthy, Nutrient regime shift in the western North Atlantic indicated by compound-specific $\delta^{15}N$ of deep-sea gorgonian corals. *Proc. Acad. Natl. Sci. U.S.A.* **108**, 1011–1015 (2011). Medline doi:10.1073/pnas.1004904108

37. H. Ehrlich, *Biological Materials of Marine Origin* (Springer, New York, 2010).

38. M. Blaauw, Methods and code for 'classical' age-modelling of radiocarbon sequences. *Quat. Geochronol.* **5**, 512–518 (2010). doi:10.1016/j.quageo.2010.01.002

39. M. Stuiver, T. F. Braziunas, Sun, ocean, climate, and atmospheric $^{14}CO_2$: An evaluation of causal and spectral relationships. *Holocene* **3**, 289–305 (1993). doi:10.1177/095968369300300401

40. P. J. Reimer, M. G. L. Baillie, E. Bard, A. Bayliss, J. W. Beck, P. G. Blackwell, C. Bronk Ramsey, C. E. Buck, G. S. Burr, R. L. Edwards, M. Friedrich, P. M. Grootes, T. P. Guilderson, I. Hajdas, T. J. Heaton, A. G. Hogg, K. A. Hughen, K. F. Kaiser, B. Kromer, F. G. McCormac, S. W. Manning, R. W. Reimer, D. A. Richards, J. R. Southon, S. Talamo, C. S. M. Turney, J. van der Plicht, C. E. Weyhenmeyer, IntCal09 and Marine09 radiocarbon age calibration curves, 0–50,000 years cal BP. *Radiocarbon* **51**, 1111–1150 (2009).

41. P. J. Reimer, E. Bard, A. Bayliss, J. W. Beck, P. G. Blackwell, C. B. Ramsey, C. E. Buck, H. Cheng, R. L. Edwards, M. Friedrich, P. M. Grootes, T. P. Guilderson, H. Haflidason, I. Hajdas, C. Hatté, T. J. Heaton, D. L. Hoffmann, A. G. Hogg, K. A. Hughen, K. F. Kaiser, B. Kromer, S. W. Manning, M. Niu, R. W. Reimer, D. A. Richards, E. M. Scott, J. R. Southon, R. A. Staff, C. S. M. Turney, J. van der Plicht, IntCal13 and Marine13 radiocarbon age calibration curves 0–50,000 years cal BP. *Radiocarbon* **55**, 1869–1887 (2013). doi:10.2458/azu_js_rc.55.16947

42. K. W. McMahon, M. L. Fogel, T. S. Elsdon, S. R. Thorrold, Carbon isotope fractionation of amino acids in fish muscle reflects biosynthesis and isotopic routing from dietary protein. *J. Anim. Ecol.* **79**, 1132–1141 (2010). Medline doi:10.1111/j.1365-2656.2010.01722.x

43. G. A. Goodfriend, Aspartic acid racemization and amino acid composition of the organic endoskeleton of the deep-water colonial anemone *Gerardia*: Determination of longevity from kinetic experiments. *Geochim. Cosmochim. Acta* **61**, 1931–1939 (1997). doi:10.1016/S0016-7037(97)00067-7

44. T. Larsen, D. L. Taylor, M. B. Leigh, D. M. O'Brien, Stable isotope fingerprinting: A novel method for identifying plant, fungal, or bacterial origins of amino acids. *Ecology* **90**, 3526–3535 (2009). Medline doi:10.1890/08-1695.1

45. J. Lehman, thesis, University of California–Santa Cruz, Santa Cruz, CA (2009).

46. M. D. McCarthy, J. Lehman, R. Kudela, Compound-specific amino acid δ^{15}N patterns in marine algae: Tracer potential for cyanobacterial vs. eukaryotic organic nitrogen sources in the ocean. *Geochim. Cosmochim. Acta* **103**, 104–120 (2013). doi:10.1016/j.gca.2012.10.037

47. J. M. Hayes, Fractionation of carbon and hydrogen isotopes in biosynthetic processes. *Rev. Mineral. Geochem.* **43**, 225–277 (2001). doi:10.2138/gsrmg.43.1.225

48. A. L. Lehninger, *Biochemistry* (Worth, New York, 1975).

49. G. N. Stephanopoulos, A. A. Aristidou, J. Nielsen, *Metabolic engineering: principles and methodologies.* (Academic Press, San Diego, CA, USA, 1998).

50. P. J. Reeds, Dispensable and indispensable amino acids for humans. *J. Nutr.* **130**, 1835S–1840S (2000). Medline

51. N. L. Vokhshoori, T. Larsen, M. D. McCarthy, Reconstructing δ^{13}C isoscapes of phytoplankton production in a coastal upwelling system with amino acid isotope values of littoral mussels. *Mar. Ecol. Prog. Ser.* **504**, 59–72 (2014). doi:10.3354/meps10746

52. E. J. Ward, B. X. Semmens, D. E. Schindler, Including source uncertainty and prior information in the analysis of stable isotope mixing models. *Environ. Sci. Technol.* **44**, 4645–4650 (2010). Medline doi:10.1021/es100053v

53. A. C. Parnell, R. Inger, S. Bearhop, A. L. Jackson, Source partitioning using stable isotopes: Coping with too much variation. *PLOS ONE* **5**, e9672 (2010). Medline doi:10.1371/journal.pone.0009672

54. R Core Team, R: A Language and Environment for Statistical Computing (R Foundation for Statistical Computing, Vienna, 2013); http://www.R-project.org/.

55. B. Fry, Alternative approaches for solving underdetermined isotope mixing models. *Mar. Ecol. Prog. Ser.* **472**, 1–13 (2013). doi:10.3354/meps10168

56. M. T. Brett, Resource polygon geometry predicts Bayesian stable isotope mixing model bias. *Mar. Ecol. Prog. Ser.* **514**, 1–12 (2014). doi:10.3354/meps11017

57. A. L. Bond, A. W. Diamond, Recent Bayesian stable-isotope mixing models are highly sensitive to variation in discrimination factors. *Ecol. Appl.* **21**, 1017–1023 (2011). Medline doi:10.1890/09-2409.1

58. A. W. Galloway, M. Eisenlord, M. Dethier, G. Holtgrieve, M. Brett, Quantitative estimates of isopod resource utilization using a Bayesian fatty acid mixing model. *Mar. Ecol. Prog. Ser.* **507**, 219–232 (2014). doi:10.3354/meps10860

59. A. W. Galloway, S. J. Taipale, M. Hiltunen, E. Peltomaa, U. Strandberg, M. T. Brett, P. Kankaala, Diet-specific biomarkers show that high-quality phytoplankton fuels herbivorous zooplankton in large boreal lakes. *Freshwater Biol.* **59**, 1902–1915 (2014). doi:10.1111/fwb.12394

60. J. I. Hedges, J. A. Baldock, Y. Gélinas, C. Lee, M. Peterson, S. G. Wakeham, Evidence for non-selective preservation of organic matter in sinking marine particles. *Nature* **409**, 801–804 (2001). Medline doi:10.1038/35057247

61. K. O. Buesseler, C. H. Lamborg, P. W. Boyd, P. J. Lam, T. W. Trull, R. R. Bidigare, J. K. Bishop, K. L. Casciotti, F. Dehairs, M. Elskens, M. Honda, D. M. Karl, D. A. Siegel, M. W. Silver, D. K. Steinberg, J. Valdes, B. Van Mooy, S. Wilson, Revisiting carbon flux through the ocean's twilight zone. *Science* **316**, 567–570 (2007). Medline doi:10.1126/science.1137959

62. B. N. Popp, B. S. Graham, R. J. Olson, C. C. S. Hannides, M. J. Lott, G. A. López-Ibarra, F. Galván-Magaña, B. Fry, Insight into the trophic ecology of yellowfin tuna, *Thunnus albacares*, from compound-specific nitrogen isotope analysis of proteinaceous amino acids. *Terr. Ecol.* **1**, 173–190 (2007). doi:10.1016/S1936-7961(07)01012-3

63. Y. Chikaraishi, Y. Kashiyama, N. O. Ogawa, H. Kitazato, N. Ohkouchi, Metabolic control of nitrogen isotope composition of amino acids in macroalgae and gastropods: Implications for aquatic food web studies. *Mar. Ecol. Prog. Ser.* **342**, 85–90 (2007). doi:10.3354/meps342085

64. Y. Chikaraishi, N. O. Ogawa, Y. Kashiyama, Y. Takano, H. Suga, A. Tomitani, H. Miyashita, H. Kitazato, N. Ohkouchi, Determination of aquatic food-web structure based

on compound-specific nitrogen isotopic composition of amino acids. *Limnol. Oceanogr. Methods* **7**, 740–750 (2009). doi:10.4319/lom.2009.7.740

65. J. W. McClelland, J. P. Montoya, Trophic relationships and the nitrogen isotopic composition of amino acids in plankton. *Ecology* **83**, 2173–2180 (2002). doi:10.1890/0012-9658(2002)083[2173:TRATNI]2.0.CO;2

66. N. L. Vokhshoori, M. D. McCarthy, Compound-specific $\delta^{15}N$ amino acid measurements in littoral mussels in the California upwelling ecosystem: A new approach to generating baseline $\delta^{15}N$ isoscapes for coastal ecosystems. *PLOS ONE* **9**, e98087 (2014). Medline doi:10.1371/journal.pone.0098087

67. K. W. McMahon, M. L. Berumen, I. Mateo, T. S. Elsdon, S. R. Thorrold, Carbon isotopes in otolith amino acids identify residency of juvenile snapper (Family: Lutjanidae) in coastal nurseries. *Coral Reefs* **30**, 1135–1145 (2011). doi:10.1007/s00338-011-0816-5

68. K. W. McMahon, M. L. Berumen, S. R. Thorrold, Linking habitat mosaics and connectivity in a coral reef seascape. *Proc. Natl. Acad. Sci. U.S.A.* **109**, 15372–15376 (2012). Medline doi:10.1073/pnas.1206378109